Optimal Design of Constant Beamwidth Beamformers with Concentric Ring Arrays

Avital Kleiman

Optimal Design of Constant Beamwidth Beamformers with Concentric Ring Arrays

Research Thesis

Submitted in partial fulfillment of the requirements
for the degree of Master of Science in Electrical Engineering

Avital Kleiman

Submitted to the Senate
of the Technion — Israel Institute of Technology
Nisan 5782 Haifa April 2022

This research was carried out under the supervision of Prof. Israel Cohen and Dr.Baruch Berdugo, in the Faculty of Electrical and Computer Engineering.

Some results in this thesis have been published as articles by the author and research collaborators in conferences and journals during the course of the author's masters research period, the most up-to-date versions of which being:

Avital Kleiman, Israel Cohen, and Baruch Berdugo. Constant-beamwidth beamforming with concentric ring arrays. *Sensors, special issue on Sensors in Indoor Positioning Systems*, 21:7253—7271, November 2021.

Avital Kleiman, Israel Cohen, and Baruch Berdugo. Constant-beamwidth nonuniform concentric ring microphone arrays. *IEEE/ACM Transactions on Audio, Speech, and Language Processing*, 2022 submitted.

Acknowledgements

This thesis was done under the supervision of Professor Israel Cohen and Dr. Baruch Berdugo in the Department of Electrical and Computer Engineering.

I would like to express my gratitude to my advisors, Professor Israel Cohen and Dr. Baruch Berdugo, for their supervision, guidance and support throughout this research. The close guidance allowed me to learn and develop new skills through this journey, and for that I am highly appreciative.

Lastly, I would like to thank my family and my partner Matan for supporting and encouraging me through this process. This accomplishment would not have been possible without them.

The generous financial support of the Technion, the ISF-NSFC joint research program (grant No. 2514/17), and the Pazy Research Foundation is gratefully acknowledged.

Contents

List of Figures

Abstract **1**

Abbreviations **3**

Notations **5**

1 Introduction **7**

1.1 Background and Motivation 7
1.2 Main Contributions 11
1.3 Research Overview 11
1.4 Organization 13

2 Preliminaries **15**

2.1 Propagating Wave Fields 15
2.2 Sensor Arrays 16
2.3 Time-Space Filtering of CRA 17
2.4 Beampattern Characteristics 20

3 Window-based Constant Beamwidth CRA **23**

3.1 Background 23
3.2 Theoretical Analysis 24
3.3 Proposed Beamformer Design 25
3.3.1 Number of Sensors 25
3.3.2 Calculating the Attenuation Coefficients 26
3.3.3 Weights Adaptation in Low Frequencies 28
3.3.4 Directivity Index Improvement 30
3.3.5 Time Domain Filter Implementation 31
3.4 Performance Analysis 33
3.4.1 Beamwidth Consistency 35
3.4.2 Directivity Index and White Noise Gain 35
3.4.3 Sidelobe Attenuation 36

3.4.4 Beamwidth Variability 37
3.5 Summary 39

4 Constant-Beamwidth Nonuniform CRAs **41**
4.1 Background 41
4.2 Array Pattern Synthesis 42
4.2.1 Optimization Constraints 43
4.2.2 Directivity Factor Maximization 45
4.2.3 Time Domain Filter Implementation 47
4.3 Experimental Results 49
4.4 Summary 52

5 Conclusions **55**
5.1 Summary 55
5.2 Future Research 57

Hebrew Abstract **i**

List of Figures

1.1 Conference room illustration with circular ceiling array covering multiple beamforming zones. 10

2.1 A three-dimensional coordinate system with Cartesian and spherical coordinates. 16

2.2 Illustration of a CRA with M rings, where $\psi_{m,k}$ indicates the angular position of the kth element on the mth ring, constructed of N_m sensor elements. 17

2.3 Block diagram of joint weights CRA beamformer. 19

2.4 Basic structure of a beampattern 21

3.1 Beampatterns of the 6-ring CRA, (**a**) without constant-beamwidth beamformer weights, and (**b**) after applying the constant-beamwidth beamformer weights. 29

3.2 Beampatterns of the 6-ring CRA, (**a**) without lower frequencies beamwidth extension, and (**b**) with the extension. The dashed line marks the amplitude in which the BW is defined $\beta_{\mathrm{BW}} \triangleq -3$ dB. 31

3.3 Constant-beamwidth beamformer for 6-ring CRA implemented with temporal FIR filters. (**a**) Weight values applied on the rings; (**b**) beampattern. 34

3.4 Beamwidth θ_{BW} as a function of frequency for different beamformers: CRA-LP (solid line with circle), EXT-CRA (dashed line with asterisks), EXT-CRA-I (dotted line with squares), and ULA (dash-dotted line with triangles). 35

3.5 Performance measures for CRA-LP (solid line with circle), EXT-CRA (dashed line with asterisks), EXT-CRA-I (dotted line with squares), and ULA (dash-dotted line with triangles): (**a**) DI, and (**b**) WNG, as a function of frequency. 36

3.6 Beampatterns at different frequencies calculated for (**a**) EXT-CRA-I, and (**b**) ULA. The first sidelobe level, the desired BW and the -3 dB amplitude are marked by a dash-point line, solid line and dotted line, respectively. 37

3.7 Beampatterns of a 6-ring CRA with several desired beamwidth specifications. The presented beampatterns are for $\theta_{\mathrm{BW}} = [20°, 30°, 40°, 50°]$, ordered from left to right. 38
3.8 (**a**) DI, and (**b**) WNG, as a function of frequency, for EXT-CRA with beamwidths: $\theta_{\mathrm{BW}} = 20°$ (solid line), $\theta_{\mathrm{BW}} = 30°$ (point-dashed line), $\theta_{\mathrm{BW}} = 40°$ (dashed line) and $\theta_{\mathrm{BW}} = 50°$ (dotted line). 39

4.1 Constant beamwidth optimized NU-CRA beamformer. (a) Chosen rings (dashed-red) out of the optional radii grid. The grid was downsampled for visualization reasons. (b) Beamformer weight values applied to the array at each frequency. 49
4.2 Beampattern of a 5-ring CRA, attenuated with the nonuniform beamformer filters. The dashed line marks the half-power (-3 dB) points of the main lobe. 50
4.3 Performance measures for 5-ring U-CRA (dash-dot line with triangles) and NU-CRA (dotted line with squares) beamformers. (a) DF and (b) WNG, as a function of frequency. The x-axis is log-scaled for presentation. 51
4.4 Performance measures for 4-ring U-CRA (dash-dot line with triangles) and NU-CRA (dotted line with squares) beamformers. (a) DF and (b) WNG, as a function of frequency. 52
4.5 Beampattern for $f = 5000$ Hz calculated for U-CRA (dash-dot line with triangles) and NU-CRA (dotted line with squares) beamformers. The first sidelobe level of each beampattern is marked by a dashed line. . . . 53

Abstract

Numerous applications require dealing with broadband signals. Acquiring acoustic data of high quality is a challenging task as the acoustic medium introduces artifacts like noise and reverberations. Thus, a wide variety of tasks, such as source separation, noise reduction, and signal enhancement, utilize wideband beamforming algorithms to mitigate possible artifacts. Implementing the desired beampattern is commonly done by changing the weights of each sensor and by choosing an adequate array geometry. Choosing the array geometry has a major impact on the performance. In three-dimensional problems, the planar geometry is preferred compared to linear geometry.

A main challenge in designing a wideband beamformer is maintaining a constant beamwidth over a wide range of frequencies. In common beamforming methods, the mainbeam becomes narrower as the frequency increases. To avoid non-uniform attenuation and distortion caused by the beamformer, several approaches implementing frequency invariant beamformers were presented in the literature. However, existing methods mostly focus on the azimuth-beamwidth. In practical 3D applications, the elevation angle is not restricted to the array plane. The assumption of arbitrary elevation angle directly affects the directivity factor and the white-noise-gain. In this thesis, we present several approaches in designing constant-elevation beamwidth beamformers on concentric ring arrays (CRAs). In the proposed configuration, all sensors on each ring share the same weight value. This constraint significantly simplifies the beamformers and reduces the resources required in a physical setup.

Based on similar approaches in one-dimensional beamformers design, a window-based constant beamwidth beamformer for CRAs is presented. By analyzing the properties of a continuous ring beampattern, we derive the relation between the beamwidth and the radius of the array. Following, the exact weight value is calculated to attain the desired beamwidth while gradually eliminating sensors from outer rings. We introduce a design method in the low-frequency range that modifies the filters applied to each array element from lowpass filters to bandpass filters. This method exploits the circular geometry and results in better performance compared to beamformers that are designed for linear arrays with an equivalent number of channels (i.e., beamformer order). A directivity index improvement and a time-domain implementation of the theoretical filters are also incorporated in the beamformer design. We demonstrate the advantages

of the proposed beamformers compared to the one-dimensional configuration in terms of different performance measures.

Following, we propose a new approach for designing constant elevation beamformers on nonuniform CRA. Opposed to common solutions that consider uniformly spaced circular arrays, the suggested methodology simultaneously selects the ring placements and designs the beamformer weights that achieve optimal performance. The the considered beamformers is designed by solving a dedicated quadric optimization problem. Hence, the suggested beamformer aims to maximize the array directivity factor while maintaining fixed beamwidth. We present the problem constraints and cost function, resulting in a sparse beamformer design. In addition, a uniformly spaced beamformer is incorporated in the optimization cost function to attain improved performance. Time-domain implementation of the ideal beamformer is also presented. Experimental results demonstrate the advantages of the nonuniform beamformer compared to a uniform beamformer.

Abbreviations

3D	:	Three-Dimensional
CRA	:	Concentric Ring Array
DF	:	Directivity Factor
DOA	:	Direction of Arrival
DRR	:	Direct-to-Reverberant Ratio
FI	:	Frequency Invariant
FIR	:	Finite Impulse Response
LP	:	Low Pass
MMSE	:	Minimum Mean-square Error
UCA	:	Uniform Circular Array
UCCA	:	Uniform Concentric Circular Arrays
ULA	:	Uniform Linear Array
WNG	:	White Noise Gain

Notations

$\mathcal{B}\left[\underline{\boldsymbol{h}}\left(f\right)\right]$	:	The designed beampattern
$\mathcal{B}_{\mathrm{p}}\left(f,R,\theta\right)$	:	Beampattern of a rigid plane piston
$\mathcal{B}_{\mathrm{r}}\left(f,r,\theta\right)$	:	Beampattern of a continuous ring
c	:	Speed of sound
$\mathcal{D}\left(f\right)$	:	Directivity factor
$\mathcal{D}_{\mathrm{u}}\left(f_j\right)$	:	Directivity factor vector
$\underline{\boldsymbol{d}}\left(f,\theta,\phi\right)$	:	Steering vector of the CRA
$\underline{\boldsymbol{d}}_m\left(f,\theta,\phi\right)$	:	Steering vector of the mth ring
f	:	Frequency
f_{H}	:	The high frequency boundary
f_{L}	:	The low frequency boundary
$f\left(t,\mathbf{r}\right)$	:	The time-space representation of a signal
$\boldsymbol{\mathcal{H}}$	:	Weight matrix
$H_m\left(f\right)$	:	The complex gain of the mth ring
$\underline{\boldsymbol{h}}\left(f\right)$	:	The beamformer coefficients vector of the CRA
$\underline{\boldsymbol{h}}_m\left(f\right)$	:	The beamformer coefficients vector of the mth ring
J	:	Number of frequency bins
J_1	:	First-order Bessel function
$\mathbf{k}$	:	Wavenumber vector
M	:	Number of rings
$\boldsymbol{\mathcal{M}}$	:	Binary mask
N	:	Number of sensors in the array
N_m	:	Number of sensors on the mth ring
N_{R}	:	Number of possible radii
R	:	Radius of a plane piston
$\underline{\boldsymbol{\mathcal{R}}}\left(f,\theta\right)$	:	Ring responses vector
$\mathcal{R}_m\left(f,\theta\right)$	:	The discrete ring response
$\underline{\boldsymbol{r}}$	:	Ring locations vector
r_m	:	Radius of the mth ring
$r_{m,k}$	:	Placement of the kth sensor on the mth ring
t	:	Time domain indication
$\mathcal{W}\left(f\right)$	:	White noise gain

$x(t)$	:	An acoustic source signal in time domain
$Y_{m,k}$	:	The signal in the output of the kth sensor on the mth ring in frequency domain
$y_{m,k}$	:	The signal arrived to the kth sensor on the mth ring
β_{BW}	:	Beamwidth amplitude
$\Gamma(f)$	:	The pseudo-coherence matrix
δ_m	:	The inner space between two adjacent sensors on the mth ring
θ	:	Elevation angle
θ_{BW}	:	The desired beamwidth
λ	:	Wavelength
ϕ	:	Azimuth angle
$\psi_{m,k}$	:	Angle of the kth sensor on the mth ring
Ω	:	Frequency space
ω	:	Angular frequency
∇^2	:	Laplacian operator
$(\cdot)^T$	:	Conjugate transpose operator
$\|\cdot\|_2$	:	The ℓ_2-norm
$\underline{\mathbf{1}}_{1\times N}$	:	The unit vector of length N

Chapter 1

Introduction

1.1 Background and Motivation

Applications in communication, radar, and speech processing require dealing with broadband signals [1]. The main purpose of these applications is to improve the quality of the signal while suppressing interferences and noises [2, 3]. A wide variety of tasks, such as source separation, noise reduction, and signal enhancement, are enhanced by utilizing sensor arrays in these applications [4, 5]. Sensor arrays are constructed of several acoustic sensors arranged in a certain geometrical form. By sampling the arriving signal with spatial diversity, the array outputs can provide various functionalities through processing. Preforming algorithms to spatially filter the input signal from a sensor array is generally reffed to as beamforming.

Common beamforming methods, like delay-and-sum [2], employ a single weight value to the entire frequency spectrum. In applications where a signal is composed of various frequency components, these beamforming methods are ineffective. Hence, many frequency invariant (FI) broadband beamformer designs were suggested in the literature over the years [6–15]. These beamformers are designed to yield a FI directivity pattern across all the bandwidth of interest, thus, the output signal is not distorted since each of its frequency components sees the same beamformer. The FI beamformers provided enhanced performances in various tasks while avoiding distortion of the signal of interest. However, most of the suggested beamformers either require more physical hardware and computational complexity or allow model mismatches errors.

In addition to the beamforming algorithm, choosing the array geometry has a major impact on the performance. Therefore, the array geometry should suit the problem specifications. In three-dimensional (3D) problems, the planar array geometry is preferred compared to the uniform linear array (ULA) geometry (which is widely used in numerous beamforming algorithms in the literature) [16–18]. Due to its symmetric geometry and the all-azimuth scan capability, the uniform circular array (UCA) geometry was the main focus among the planar array beamformer designs presented in the last decade. Uniform concentric circular arrays (UCCAs), constructed of multiple rings,

exhibited superior performance in terms of the direction of arrival (DOA) estimation, broadband beamforming, and noise suppression [19–23]. Thus, in applications where the signal of interest may come from any direction, circular arrays are advantageous.

Due to the progress in audio and communication applications, many beamforming methods were proposed for UCCAs over the last decade. A common criterion in designing an FI beampattern is the minimum mean-square error (MMSE). By minimizing the mismatched error between the synthesized and desired beampattern, the optimal beamforming solution is computed. This approach for UCCAs was suggested in [24], and was later incorporated in [25,26] as an optimization cost function subject to different problem constraints. The employment of convex optimization to attain broadband fixed pattern was also suggested in [27], formulating a second-order cone programming problem. The optimized solution presented better performance compared to conventional beamformers and required fewer adaptive parameters. Thus, the proposed method was later modified to 3D spherical arrays, in [28]. Utilizing convex optimization methods to attain the desired beampattern on circular geometry was also presented in [25, 29–31]. These beamforming algorithms focused on sparse beamformers, minimizing the number of sensors while attaining FI beampattern. A greedy-based sparse design was introduced, optimizing simultaneously the number of rings and the number of sensors in the array. Hence, the results yielded an optimal solution on sparse array layouts. Recently, the use of differential sensor arrays on the circular geometry was investigated in [32–36]. Differential sensor array refers to arrays that combine closely spaced sensors to respond to the spatial derivatives of the acoustic pressure field. Incorporating differential arrays in the circular geometry provided enhanced performance in terms of steering flexibility and beampatterns irregularities.

In spite of the presented benefits, the suggested beamformers obtain several disadvantages:

- Most of the UCCA FI beamformers consider the scenario in which the signal-of-interest arrives from the horizontal plane. However, in practical 3D applications, the elevation angle is not restricted to 90°. The assumption of arbitrary elevation angle directly affects the directivity factor (DF) and the white-noise-gain (WNG), important performance measures of the array. In addition, solutions derived under this condition may not generalize well to more practical scenarios where the signal-of-interest impinges on the UCCA at an arbitrary oblique elevation angle.

- The presented beamformers consider individual weight values applied on each sensor separately. While providing steering capability, in the aspect of a physical set-up this assumption may require more hardware and computational resources compared to beamformers with reduced degrees of freedom.

- The beamformer design mostly focuses on minimizing the MMSE between the

desired beampattern and the actual beampattern over a range of frequencies. Relaxing the restriction of the desired beampattern outside the main lobe potentially provides superior performance in terms of beamwidth consistency, computational complexity, and the number of physical resources required in the setup [37–39].

A common approach for designing a FI beamformer is focusing on maintaining fixed mainbeam width. That is, beamformers that have a constant beamwidth over a wide range of frequencies, referred to as constant beamwidth beamformers. As mentioned above, conventional beamformers apply different spatial filters in different frequencies, which results in narrowing the mainlobe as the frequency increases. As a result, there is an inverse dependency between the beamwidth and frequency. Note that the FI beamformers on UCCAs are utilized for the design of general broadband beamformers and not necessarily for designing constant beamwidth beamformers. The task of beamforming and constant beamwidth beamforming, in particular, remains a major challenge, especially on planar arrays. Several constant beamwidth beamformers were suggested in the literature for ULAs [40–43]. These methods examined the beampattern characteristics as a function of frequency and applied spatial window function to attain constant beamwidth over a range of frequencies. Recently, constant beamwidth beamformers for UCCAs were presented in [44, 45], enabling control of the elevation and azimuth beamwidth by weighting the sensors on each ring. The sensor weighting considered the alignment of each sensor with the signal path and its corresponding ring position.

Constant elevation beamformers can be incorporated in a system of circular ceiling arrays, Covering multiple beamforming zones. This solution can be used in scenarios of multi-speakers settings, such as large conference rooms, auditoriums, and lecture halls. There are several types of beamforming technologies for designing ceiling sensor arrays. The dynamic beamforming approach adaptively steers the mainbeam to the desired speaker direction. The steering is performed by separately sampling each sensor element and applying individual complex weight to each sensor. While there are advantages to adaptive beamforming, such as flexibility in the speaker locations, it usually requires more hardware resources or higher computational complexity. In addition, adaptive beamformers are used to steer the mainbeam to focus on the current speaker. Hence, the performance of such beamformers in practical environments depends on the direct-to-reverberant ratio (DRR) and the speakers' distance from the array [46,47]. Moreover, planar arrays are usually constructed of a large number of elements. A multichannel beamforming design that steers the beam adaptively requires a significant number of phase shifters, amplifiers, samplers, and filters. The physical hardware affects the array cost, maintenance, sensitivities to model mismatches, diversity of sensors, and deviation from nominal configuration [48].

Developing ceiling sensor arrays with multiple fixed beam-forming zones that incorporate predetermined recording regions is a way of eliminating the need for beam

Figure 1.1: Conference room illustration with circular ceiling array covering multiple beamforming zones.

steering. Given a room layout and a number of ceiling circular arrays, one can cover the area of interest by combining several fixed beamformers with designated beamwidth as demonstrated in Fig. 1.1. Each signal in the scope of the main beam arrives at the closest array from the broadside with a certain elevation angle.

A system of this type offers the following benefits:

- **Fixed beam direction**: as the source signal is assumed to be within the area covered by the main lobe, there is no need to estimate the source location and steer the beam to the estimated direction.

- **Low resource setup:** by eliminating the need of steering the beam, the proposed design enables the use of fewer A/D samplers, phase shifters, and filters, which is significant in 2D arrays. In the proposed system, all sensors on each ring share joint weights. As a result, an analog summation of all the received signals from a given ring before sampling is allowed.

- **Real-time processing:** since the number of channels in each array is determined by the number of rings (rather than the number of sensors), the beamformer includes fewer filters, has lower computational complexity, and the processing time is faster.

The redundancy of beam-steering in the presented fixed beamformers system permits the use of concentric ring array (CRAs) rather than UCCAs. That is, one can restrict all the sensors on each ring to have the same weights. This restriction allows a significant improvement in computational complexity since the number of weights is

determined by the number of rings in the array, rather than the number of sensors. In addition, designing joint weights for all the sensors on a given ring enables an analog summation of the sensors' signals before sampling. Accordingly, this design enables to use a single A/D sampler per ring, instead of sampling each sensor individually. In this thesis, constant-elevation beamwidth beamformers are presented. The beamformers are designed for CRA and can be incorporated in a multi-beam system described above.

1.2 Main Contributions

In light of the above-stated drawbacks, this research is focused on several practical design aspects of constant-elevation beamwidth beamformers, applied on CRAs. In the presented work, there are several main contributions to this research:

- A new window-based constant elevation beamformer is suggested, based on a gradual elimination process of outer rings. The proposed elimination maintains fixed beamwidth over a wide range of frequencies. The beamformer weights are calculated in exact form, based on the beampattern characteristics of the array.
- By analyzing the geometrical properties of the CRA, a low-frequency modification is proposed - enlarging the bandwidth for which the beamwidth is attained. An improved directivity index design in frequencies lower than the range limits is also implemented.
- A sparse design of nonuniform CRA is considered, aiming to optimize the directivity factor while maintaining constant elevation beamwidth. The beamformer obtains superior performance in terms of directivity factor, beamwidth consistency, and robustness. A uniformly spaced beamformer is incorporated in the optimization cost function to attain improved performance.
- The proposed beamformers apply the same filter to all the elements on each ring. This constraint lowers computational complexity in design and enables a physical setup that requires fewer resources.

In the remainder of this chapter, we describe two beamformers and indicate the design considerations that motivated the proposed methods.

1.3 Research Overview

The presented research addresses the design of CRA beamformers, with constant elevation beamwidth. The primary goal is to maintain a fixed beamwidth over a wide range of frequencies, under the joint weights constraint. In the suggested methods, different degrees of freedom in the design are considered.

First, a window-based beamformer is proposed. We assume a linearly spaced CRA, with pre-defined radii. By analyzing the characteristics of the beampattern of a continuous CRA and a planar piston, a gradual elimination method is suggested. Thus, the theoretical relation between the effective radius of the array and the frequency is deployed. Relying on the frequency-radius correspondence, we suggest a new method to maintain a constant beamwidth. The design is based on a similar method proposed in [42], adjusted to the 2-D scenario. The attenuation coefficients are calculated analytically and a precise form of the beamformers weights is presented. By gradually attenuating the outer rings as the frequency increases, the resulting beampattern obtains FI beamwidth over a wide range of frequencies. Moreover, we utilize the geometrical properties of the array to extend the frequency range for which a constant beamwidth is achieved. Hence, the filters applied on each ring in the array are modified from low pass filters to bandpass filters. In addition, we suggest another modification in lower frequencies to improve the array performance. Integrating the two outer-most rings in the beamforming process in out-of-range frequencies yields a higher directivity factor compared to the original design. The advantages of the proposed beamformer are demonstrated in terms of DI, WNG, beamwidth consistency, and sidelobe attenuation compared to a 1-dimensional ULA with an equivalent number of channels. Furthermore, the ability of the proposed beamformer to support variable desired beamwidth is also shown. That is, the beamformers' competence to attain various beamwidths (under a constant ring constellation and number of sensors) is examined. The simplicity of the suggested beamformer is the main advantage since it is reflected in low computational complexity and practical advantages in physical setups.

An important aspect of designing a beamformer is the geometrical layout of the array. While the window-based approach yields an efficient constant beamwidth beamformer, it does not include optimization of the ring constellation. Thus, we extend the following research to discuss constant beamwidth CRAs with nonuniform ring spacing. The proposed methodology performs two actions: A selection of rings spacing out of a given radii grid and a design of the beamformers weights. The suggested beamformer aims to maximize the array directivity factor while maintaining fixed beamwidth over a wide range of frequencies. To do so, we define a quadric programming optimization problem [49] over the entire frequency range. In the presented beamformer we specify the problem constraints and cost function. The suggested constraints objective is to maintain a fixed beamwidth, control the array response in the signals' direction-of-arrival, and select the ring placements. Simultaneously, the problems' cost function is defined to maximize the DI of the array. Hence, the optimal solution is chosen from a rigid grid of possible radii and performed coherently over all the frequency bins. Since the ring locations should be consistent for all frequencies, the optimization is performed over the entire frequency band. In addition, to enforce the desired radii selection for all the frequencies in the range we introduce a binary mask variable. Moreover, we introduce an additional beamformer applied on a linearly spaced CRA with an equal

number of rings. The uniform beamformer is designed by solving an equivalent optimization problem. Since the ring spacing is pre-defined, the optimization is performed for each frequency bin individually. The uniform beamformer is later used as a weighting function, incorporated in the nonuniform cost function. That is, to outperform the uniform beamformer the DF of the resulting uniform beamformer is used as a weighting coefficient for the nonuniform beamformer cost function. The superior performance of the nonuniform beamformer compared to the uniform beamformer will be presented in this research. Furthermore, we show the beamformers' performance measures given different numbers of rings in the array. In the case of fewer rings, the nonuniform beamformers' advantages are emphasized.

In a physical setup, the beamformer filters are implemented through temporal finite impulse response (FIR) filters. As a result, in both of the suggested beamformers, a time-domain implementation of the ideal beamformer filters is presented. We determine the temporal FIR filter coefficients by approximating the resulted beamformer response to the ideal beamformer. As will be presented following, we introduce different methods to minimize the number of required filter taps to decrease the number of resources required in a physical set-up. Nonetheless, as specified above all the described beamformers are performed on CRA. Accordingly, the designs enable the use of a single A/D sampler per ring, requiring a significantly lower number of hardware resources and maintenance costs in real-life applications.

1.4 Organization

This thesis is organized as follows. In Chapter 2 we present the scientific background related to this work. We also present the problem formulation and the discussed array constellation. The original contribution of this research starts in Chapter 3, where a window-based constant beamwidth beamformer is suggested for CRAs. A novel design is suggested based on analysis of the theoretical beampattern characteristics and the performance is evaluated compared to a linear array. In Chapter 4, an additional design methodology is presented, which simultaneously selects the optimal ring placements and the applied weight for each frequency. Experimental results show the enhanced performance of the suggested non-uniform beamformer compared to a uniform CRA. Chapter 5 concludes and summarizes the main contributions of this thesis and presents some future research directions.

Chapter 2

Preliminaries

In this chapter, we provide some background for reading this thesis and briefly describe relevant methods and metrics used in the research. First, the fundamentals of wave propagation are described in Section 2.1. Following, Section 2.2 provides an overview of array processing and presents the circular array geometry. We also introduce in Section 2.3 the processing of the spatially sampled impinging wave signals by the sensors array. In this section, the problem formulation is presented for a CRA with joint weights for all the sensors on each ring. Finally, in Section 2.4 the basic components of the array directivity pattern are shown. Furthermore, the performance measures used for the beamformers evaluations are described.

2.1 Propagating Wave Fields

Array Processing involves the use of multiple sensors to receive or transmit a signal. Considering microphone arrays applications, the received signal is an acoustic signal propagating in the speed of sound. Let $f(t, \mathbf{r})$ denote the time-space representation of the input signal. That is, the time domain is represented by t and the space domain is represented by a 3-D coordinates system. The spatial location can be noted by the Cartesian coordinates (x, y, z) or the three dimensional spherical coordinates (r, θ, ϕ), where $0 \leq \phi \leq 2\pi$, $0 \leq \theta \leq \pi$ are the azimuth and elevation angles, respectively. The relations between the Cartesian and spherical coordinates are given in Fig. 2.1.

In a homogeneous, dispersion free and lossless medium the wave equation can be written as:

$$\nabla^2 f(t, \mathbf{r}) - \frac{1}{c^2} \frac{\partial^2}{\partial t^2} f(t, \mathbf{r}) = 0\,, \tag{2.1}$$

where c is the speed of propagation (approximately 340 m/s for acoustic signals propagating in the air), and ∇^2 denotes the Laplacian operator. A solution to Equation

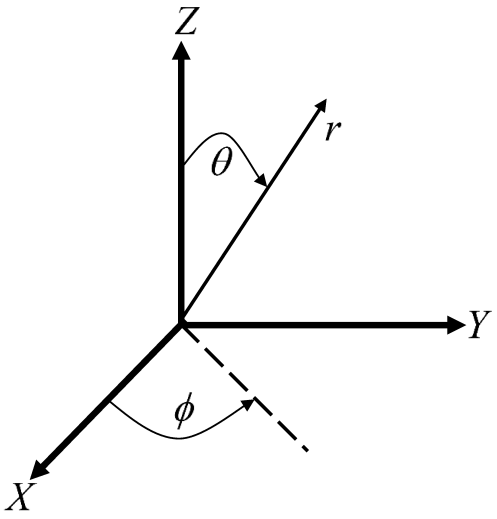

Figure 2.1: A three-dimensional coordinate system with Cartesian and spherical coordinates.

(2.1) for a plane wave can be written as:

$$f\left(t, \mathbf{r}\right) = Ae^{j(\omega t - \mathbf{k}\cdot\mathbf{r})}\,, \tag{2.2}$$

where A is a complex constant marking the wave amplitude, $\omega = 2\pi f$ is the temporal frequency and $\mathbf{k}$ denotes the *wavenumber vector*. The wavenumber vector indicates the direction of wave propagation and is given as

$$\mathbf{k} = \frac{2\pi}{\lambda}\left[\sin\theta\cos\phi \;\; \sin\theta\sin\phi \;\; \cos\theta\right]\,. \tag{2.3}$$

The constant λ denotes the distance the plane wave propagated during a single temporal period $T = \frac{2\pi}{\omega}$. The wavelength is related to the speed of propagation by $\lambda = c/f$.

2.2 Sensor Arrays

A sensor array refers to a group of independently positioned sensors, used for collecting and processing electromagnetic or acoustic signals. Each sensor samples temporally the impinging signals, which enables improved performance compared to using a single sensor. Using array signal processing, the temporal and spatial properties of the impinging signals interfered by noise and hidden in the data collected by the sensor array can be estimated and revealed. Thus, sensor arrays are used for solving numerous signal processing problems, ranging from source localization, communication, seismology, astronomy, etc.

There are several aspects to be considered when designing a sensor array such as the physical characteristics, hardware restrictions, desired application, and performance

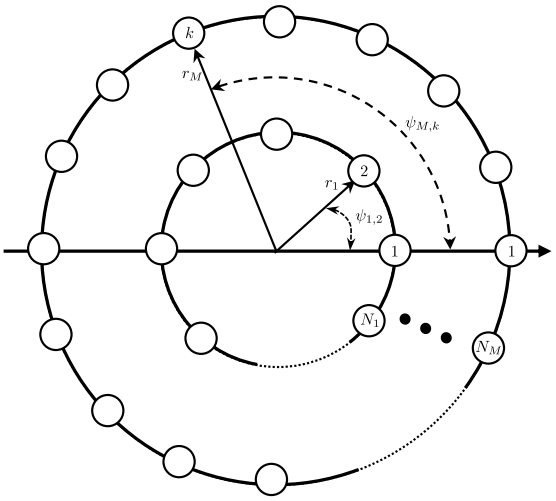

Figure 2.2: Illustration of a CRA with M rings, where $\psi_{m,k}$ indicates the angular position of the kth element on the mth ring, constructed of N_m sensor elements.

measures. Selecting the geometry of the array has a major impact on the arrays' operation and physical constraints of the design. Therefore, the array geometry should suit the problem specifications. Sensor arrays have different geometrical designs, including linear, circular, planar, cylindrical, and spherical arrays. This work is based on circular arrays and therefore we elaborate on this geometry.

The basic circular array is constructed of equally spaced omnidirectional sensor elements on each ring. In this work, we consider a CRA composed of M rings, containing N_m ($m = 1, 2, \ldots, M$) sensors in each ring, and receiving a source signal in the farfield (steered to broadside) as shown in Fig. 2.2.

Given a ring with radius r_m, the placement of the kth sensor ($k \in [1, N_m]$) on a Cartesian coordinate system is given by:

$$r_{m,k} = r_m \left(\cos \psi_{m,k}, \sin \psi_{m,k}, 0\right) , \tag{2.4}$$

where $\psi_{m,k}$ is the angle of the kth sensor on the mth ring, measured anti-clockwise from the x-axis:

$$\psi_{m,k} = \frac{2\pi \left(k-1\right)}{N_m} . \tag{2.5}$$

2.3 Time-Space Filtering of CRA

As presented in Chapter 1, sensor arrays are used in beamforming applications, spatially filtering the input signals. Given a temporal sample at time t, the measurements of the sensor array's elements are fused together and processed. The underlying spatial information is extracted using the relations between samples. The spatial response of the array is obtained by enhancing signals from certain directions while suppressing

other signals from unwanted directions, forming a beam in the desired direction.

Considering a farfield broadband plane wave $x(t)$ impinging the CRA from direction (θ, ϕ), where ϕ is the azimuth angle and θ is the elevation angle, the signal arriving at any microphone can be represented as

$$y_{m,k}(t) = x(t - \tau_{m,k}) \ , \tag{2.6}$$

$$\tau_{m,k} = \frac{r_m \sin\theta \cos(\phi - \psi_{m,k})}{\mathrm{c}} \ , \tag{2.7}$$

where c is the signal propagation speed, i.e., $340\frac{\mathrm{m}}{\mathrm{s}}$ for speech signals propagating in the air. The beamformers output is constructed as a weighted output of the sampled signals, attenuated with complex weight values.

When defining the problem in the frequency domain, the time delay is translated to a phase shift. Thus, the signal model is given by

$$Y_{m,k}(f) = \mathrm{e}^{-\mathrm{j}2\pi f \tau_{m,k}} X(f) \ , \tag{2.8}$$

where f is the temporal frequency and j is the imaginary unit with $\mathrm{j}^2 = -1$. Collecting all the data received across all the microphones of the m^{th} ring, we get

$$\begin{aligned} \underline{\boldsymbol{Y}}_m(f) &= [Y_{m,1}(f), Y_{m,2}(f), ..., Y_{m,N_m}(f)] \\ &= \underline{\boldsymbol{d}}_m(f, \theta, \phi) X(f) \ , \end{aligned} \tag{2.9}$$

where $\underline{\boldsymbol{d}}_m(f, \theta, \phi)$ is the steering vector of the m^{th} ring:

$$\underline{\boldsymbol{d}}_m(f, \theta, \phi) \triangleq \begin{bmatrix} \mathrm{e}^{\mathrm{j}\frac{2\pi r_m f}{\mathrm{c}}\cos(\phi - \psi_{m,1})\sin\theta} \\ \mathrm{e}^{\mathrm{j}\frac{2\pi r_m f}{\mathrm{c}}\cos(\phi - \psi_{m,2})\sin\theta} \\ \vdots \\ \mathrm{e}^{\mathrm{j}\frac{2\pi r_m f}{\mathrm{c}}\cos\left(\phi - \psi_{m,N_m}\right)\sin\theta} \end{bmatrix} . \tag{2.10}$$

We can describe the CRA steering vector by concatenating the M rings steering vectors:

$$\underline{\boldsymbol{d}}(f, \theta, \phi) = \left[\underline{\boldsymbol{d}}_1^T(f, \theta, \phi), ..., \underline{\boldsymbol{d}}_M^T(f, \theta, \phi)\right]^T \ , \tag{2.11}$$

where ^{T} denotes the conjugate transpose operator.

In the proposed CRA beamformer design, all the sensors in the mth ring are multiplied by the same weight value (in a given frequency f), denoted by $H_m(f)$. Designing the beampattern under this constraint provides two main advantages in practical applications. First, the computational complexity of designing the beamformer weights is significantly lower. Second, designing joint weights for all the sensors on a given ring enables an analog summation of the sensors' signals before sampling. In physical systems, this design enables the use of a single A/D sampler per ring, instead of sampling each sensor signal individually, which simplifies the required hardware. A block

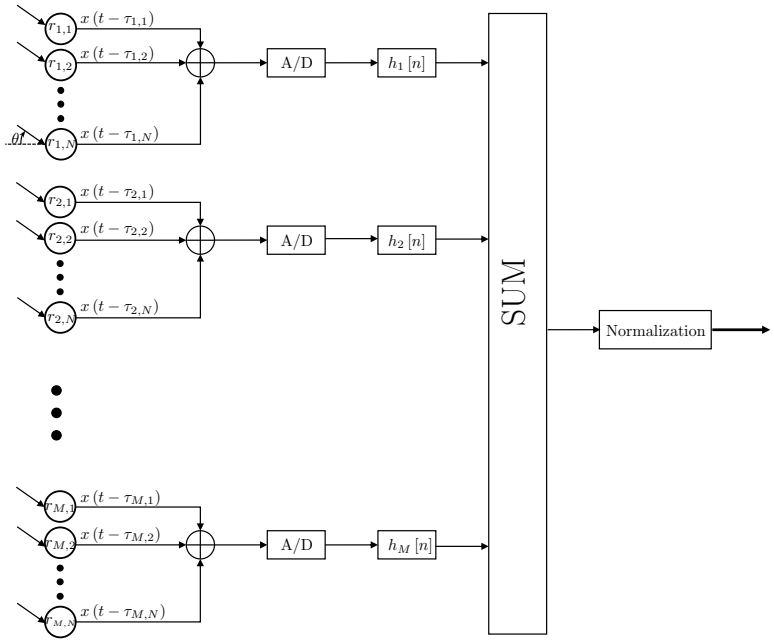

Figure 2.3: Block diagram of joint weights CRA beamformer.

diagram of the proposed design is provided in Fig. 2.3.

A source signal arriving in angle θ to the circular array is delayed by $\tau_{m,k}$ according to the sensor placements. The output signals are summed per-ring and sampled. Afterwards, each ring response is filtered by the temporal filters denoted by $h_m[n]$, where $m \in [1, M]$. The filter results are later summed and normalized by a normalization filter to yield the output signal.

Given this design restriction, the weigh vector of the mth ring is given by:

$$\underline{\boldsymbol{h}}_m(f) = H_m(f)\,\underline{\mathbf{1}}_{1\times N_m}\,, \tag{2.12}$$

where $\underline{\mathbf{1}}_{1\times N_m}$ is the unit vector of length N_m. Let $N \triangleq \sum_{m=1}^{M} N_m$ denote the total number of sensors in the array. Concatenating all the weight vectors into an $(N \times 1)$ vector, representing the weights applied on the array elements at frequency f, we obtain

$$\underline{\boldsymbol{h}}(f) = [\underline{\boldsymbol{h}}_1(f), ..., \underline{\boldsymbol{h}}_M(f)]^T\,. \tag{2.13}$$

The summation of all the weighted output signals yields the CRA beampattern, i.e.,

$$\begin{aligned}\mathcal{B}[\underline{\boldsymbol{h}}(f), \theta, \phi] &= \underline{\boldsymbol{h}}^T(f)\,\underline{\boldsymbol{d}}(f, \theta, \phi) \\ &= \sum_{m=1}^{M} H_m(f) \sum_{k=1}^{N_m} \mathrm{e}^{\mathrm{j}\frac{2\pi r_m f}{\mathrm{c}}\cos\left(\phi-\psi_{m,k}\right)\sin\theta}\,.\end{aligned} \tag{2.14}$$

A property of the discrete CRA array factor shows that with sufficient numbers of microphones on the rings, the beam pattern of the m^{th} ring is equivalent to a continuous ring of the same radius [50]. The continuous ring beampattern can be approximated

by a zero-order Bessel function and is independent of the azimuth angle ϕ [51]. As a result, without loss of generality one can choose $\phi \stackrel{\triangle}{=} 0$, which yields

$$\mathcal{B}\left(\underline{\boldsymbol{h}}\left(f\right),\theta\right) = \sum_{m=1}^{M} H_m\left(f\right) N_m \mathcal{R}_m\left(f,\theta\right) , \tag{2.15}$$

where

$$\mathcal{R}_m\left(f,\theta\right) = \frac{1}{N_m} \sum_{k=1}^{N_m} \mathrm{e}^{j\frac{2\pi r_m f}{\mathrm{c}} \cos\psi_{m,k} \sin\theta} \tag{2.16}$$

denotes the discrete ring response. In the next two subsections, we discuss some performance measures taken into consideration when designing beamformers.

2.4 Beampattern Characteristics

Each beamformer is designed to serve different requirements, based on the set-up and application. Thus, measuring the array performance depends on the problem specification. In this work, the suggested beamformers aim to maintain a constant elevation beamwidth. In addition, the nonuniform design attempts to also maximize the directivity factor of the array. Hence, to analyze the presented methods, we use related performance metrics.

The beampattern or directivity pattern describes the sensitivity of the beamformer to a plane wave (source signal) impinging on the array from the direction of arrival. We showed in Section 2.3 the mathematical representation of the array beampattern and Fig. 2.4 presents the basic structure of a beampattern. Note that the main beam refers to the central region defined in-between the -3dB amplitude. Hence, at the beamwidth angle, the main beam decreases 3dB with respect to the maximal value. The sidelobe power can be helpful in attenuating signals from out-of-beamwidth directions. Doing so can attenuate undesirable inferences and noise from the beamformers' output signal. Hence, one of the measures used to measure the array performance is the sidelobe attenuation.

Another common measure of performance of an array or aperture is the directivity factor. The DF is is an important characteristic of any beamformer [52]. Hence, one of the main goals of the beamformers proposed is to maximize the DF of the CRAs. The DF denotes the relative power between the beampattern in the direction-of-interest $(\theta_{\mathrm{d}}, \phi_{\mathrm{d}})$ with respect to the entire 3-D beampattern. The DF can be interpreted as the beamformer's ability to suppress spatial noise from directions other than the look

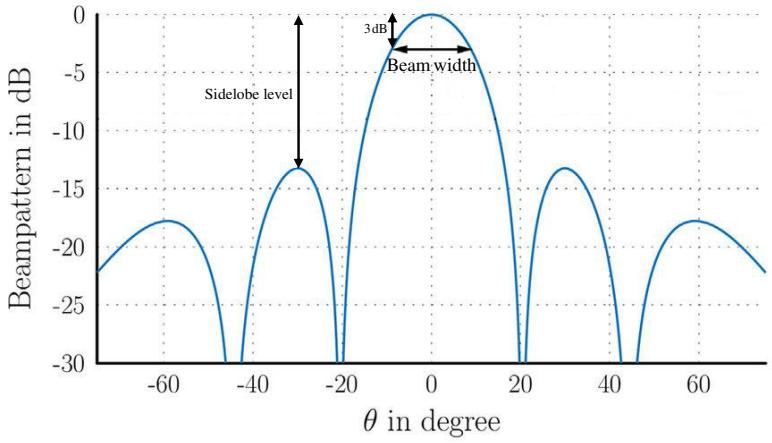

Figure 2.4: Basic structure of a beampattern

direction. The DF can be written as [2]

$$\begin{aligned}\mathcal{D}(f) &= \frac{|\mathcal{B}(f,\theta_{\mathrm{d}},\phi_{\mathrm{d}})|^2}{\frac{1}{4\pi}\int_0^{\pi}\int_0^{2\pi}|\mathcal{B}(f,\theta,\phi)|^2\sin\theta d\phi d\theta} \\ &= \frac{\left|\underline{\boldsymbol{h}}^T(f)\,\underline{\boldsymbol{d}}(f,\theta_{\mathrm{d}},\phi_{\mathrm{d}})\right|^2}{\underline{\boldsymbol{h}}^T(f)\,\Gamma(f)\,\underline{\boldsymbol{h}}(f)},\end{aligned} \tag{2.17}$$

where $\Gamma(f)$ is the pseudo-coherence matrix whose elements are

$$\Gamma_{i,j}(f) = \mathrm{sinc}\left(\frac{2\pi f\delta_{i,j}}{\mathrm{c}}\right), \tag{2.18}$$

where $\delta_{i,j}$ $1 \leq i,j \leq N$ is the Euclidean distance between two microphones, i and j, in the array.

An additional performance measure is the white noise gain, which is a measure of the array gain in a spatially uncorrelated noise environment. The WNG is an indicator of the beamformer robustness to microphones imperfections and is calculated by

$$\mathcal{W}(f) = \frac{\left|\underline{\boldsymbol{h}}^T(f)\,\underline{\boldsymbol{d}}(f,\theta_{\mathrm{d}},\phi_{\mathrm{d}})\right|^2}{\underline{\boldsymbol{h}}^T(f)\,\underline{\boldsymbol{h}}(f)}. \tag{2.19}$$

Chapter 3

Window-based Constant Beamwidth CRA

In this chapter, a constant-elevation beamwidth CRA beamformer is presented. We begin with a background on the presented methodology in Section 3.1. In Section 3.2, a theoretical justification for the suggested design is provided. The theoretical justification is based on the beampattern characteristics of the continuous ring array. Section 3.3 introduces the design method of the constant-beamwidth CRA, including a particular consideration to low frequencies and a time-domain implementation of the desired beamformer filters. Section 3.4 evaluates the performance of the proposed beamformer compared to a constant-beamwidth beamformer, of the same order that is designed for ULAs. The ability of the proposed beamformer to support various beamwidths is also examined. Finally, we conclude the window-based CRA beamformer research chapter and discuss future research in Section 3.5.

3.1 Background

We present beamformers with constant elevation beamwidth, covering a pre-defined area of interest. The pre-configured locations of the sensors in the array eliminate the need for beam steering. The weight given to each sensor is derived from theoretical considerations. The exact weight value is calculated to attain the desired beamwidth while gradually eliminating sensors from outer rings. In the design process, we utilize concentric ring arrays (CRAs). That is, we restrict all the sensors on each ring to have the same weights. This restriction allows a significant improvement in computational complexity since the number of weights is determined by the number of rings in the array, rather than the number of sensors.

Our design follows the approach proposed by Rosen et al. [42]. This method demonstrated low computational complexity as well as improved array response results in various scenarios, compared to other methods in the field. The proposed approach utilizes custom-tailored filters for each sensor, manipulating the beampattern beamwidth to

remain constant. The basic idea of the suggested algorithm includes a gradual elimination of active sensors to achieve the desired constant beamwidth in different frequencies. The elimination of the sensors is done by attenuating their signals as the frequency increases. This changes the effective aperture of the array and results in beamwidth consistency. According to this approach, each sensor output is processed by a lowpass filter with different cutoff frequencies, depending on the sensor position. In between the cutoff frequencies, smoothing magnitude coefficients are calculated such that the beamwidth remains constant. In addition, a post-summation normalization is applied to the output result, so the gain at all the frequencies is also constant. This method showed better sidelobe attenuation and robustness to array mismatches compared to other methods.

3.2 Theoretical Analysis

In order to design a constant-beamwidth beampattern for CRA, our suggested beamformer includes a gradual elimination of the outer rings in the array as the frequency increases. In this section, we provide a theoretical justification to the proposed approach by analyzing the nature of the beampattern for continuous CRA geometry.

Let us first examine the beampattern of a rigid plane piston which is dependent on the temporal frequency f, the piston radius R and the signal elevation angle θ as follows [51]

$$\mathcal{B}_{\mathrm{p}}\left(f,R,\theta\right)=\frac{J_1\left(\frac{2\pi f}{c}R\sin\theta\right)}{\frac{\pi f}{c}R\sin\theta}\,, \tag{3.1}$$

where J_1 is the first-order Bessel function. Note that due to the symmetry of the problem, the beampattern does not depend on the azimuth angle.

Let θ_{BW} define the desired beamwidth, achieved in the -3 dB amplitude of the beampattern and denoted as $\beta_{\mathrm{BW}}\triangleq 0.7$. The constant-beamwidth constraint in a given frequency range defined by $[f_{\mathrm{L}},f_{\mathrm{H}}]$ implies that:

$$\forall f\in[f_{\mathrm{L}},f_{\mathrm{H}}]:\ \mathcal{B}_{\mathrm{p}}\left(f,R,\frac{\theta_{\mathrm{BW}}}{2}\right)=\beta_{\mathrm{BW}}\,. \tag{3.2}$$

Using the beampattern defined in (3.1), we obtain

$$\frac{2\pi f}{c}R\sin\left(\frac{\theta_{\mathrm{BW}}}{2}\right)\approx 1.638\,. \tag{3.3}$$

Since we aim to keep the beamwidth constant, the value of $\sin\left(\frac{\theta_{\mathrm{BW}}}{2}\right)$ should not change over a wide range of frequencies. This can be achieved if the value of the product fR is kept constant. Hence, decreasing the piston radius as the frequency increases yields a constant beamwidth.

The CRA geometry contains concentric rings, which effectively sample the piston in discrete radii. The beampattern of a continuous circular ring laying in the x-y plane is:

$$\mathcal{B}_{\mathrm{r}}\left(f, r, \theta\right) = J_0\left(\frac{2\pi f}{c} r \sin\theta\right), \tag{3.4}$$

where J_0 is the zero-order Bessel function and r is the ring radius [51]. Note that similarly to (3.3), the beamwidth of the beampattern in (3.4) depends on the frequency and ring radius. Hence, as seen in the piston beampattern, to achieve a constant beamwidth, we need to establish a constant fr relation.

Given a CRA constructed from M concentric rings, the beampattern will be a weighted sum of the beampatterns shown in (3.4):

$$\mathcal{B}\left(f, \underline{\mathrm{r}}, \theta\right) = \sum_{m=1}^{M} H_m\left(f\right) J_0\left(\frac{2\pi f}{c} r_m \sin\theta\right), \tag{3.5}$$

where $H_m\left(f\right)$ denotes the weight given to the m-th ring in the frequency f and $\underline{\mathrm{r}} \triangleq [r_1, \ldots, r_M]$ is the radii vector of the CRA rings. By changing the weights given to each ring as the frequency increases, we can control the effective radius of the sampled piston such that the beamwidth will remain constant, as discussed above. In the following section, the beamformers' design is presented, relying on the radius–frequency relation with a gradual decrease of the effective radius.

3.3 Proposed Beamformer Design

As discussed in Section 3.2, the beamwidth of the CRA remains constant if we ensure that the radius–frequency product is constant. Thus, in this section, we suggest a beamformer design that involves the elimination of the outer rings in the CRA as the frequency increases. We also explain the geometric considerations in choosing the number of sensors constructing the array.

All the results shown in this section and in Section 3.4 are for a CRA constructed of $M = 6$ rings with radii $\underline{\mathrm{r}} = [2.5, 5, 10, 15, 20, 25]$ cm having 16 sensors each and a desired beamwidth of $\theta_{\mathrm{BW}} = 30°$. Note that even though the array contains a large number of elements, the number of weights calculated per frequency is determined by the number of rings. For simplicity, the shown results are for a broadside array. The CRA structure and problem formulation are provided in Section 2.2 of this thesis.

3.3.1 Number of Sensors

As mentioned in Section 2.3, the array is constructed of equally spaced discrete sensor elements. To avoid spatial aliasing, the spacing between the elements should be smaller than half of the wavelength λ [51]. Assuming that the sensor placement is uniform on

each ring, the inner spacing should satisfy:

$$\delta_m = 2r_m \sin\left(\frac{\pi}{N_m}\right) \approx \frac{2\pi r_m}{N_m} < \frac{c}{2f}\,, \tag{3.6}$$

where δ_m is the inner space between two adjacent sensors. Let r_{out} denote the radius of the outermost effective ring, satisfying $H_{\text{out}}(f) \neq 0$. From (3.6), the number of sensors on the outer ring in a given frequency f should comply with

$$N_{\text{out}} > \frac{4\pi r_{\text{out}} f}{c}\,. \tag{3.7}$$

Since we attenuate the outer rings as the frequency increases, r_{out} is smaller for higher frequencies. Thus, the relation $r_{\text{out}} f$ remains constant. Consequently, the right side of the inequality is constant for a wide range of frequencies. This implies that the number of elements N_{out} should not change when decreasing the effective radius. As a result, the number of sensors should be constant for all the rings in the CRA.

Equation (3.3) presents the relation between the radius–frequency product and the desired beamwidth for a rigid piston beampattern:

$$fR \approx \frac{1.638c}{2\pi \sin\left(\frac{\theta_{\text{BW}}}{2}\right)}. \tag{3.8}$$

Substituting fR into (3.7) yields the following dependency between the number of sensors and the desired beamwidth

$$N > \frac{4\pi}{c} \frac{1.638c}{2\pi \sin\left(\frac{\theta_{\text{BW}}}{2}\right)} = \frac{3.276}{\sin\left(\frac{\theta_{\text{BW}}}{2}\right)}. \tag{3.9}$$

Under the chosen beamwidth restriction, we have $N > 12.7$. To verify that the chosen number of discrete sensor elements in the CRA is sufficient, we examine the discretization error between the continuous ring CRA beampattern and the discrete CRA in the following manner:

$$\varepsilon = \max_{f,\theta} \left| \sum_{m=1}^{M} H_m(f) \left[\mathcal{R}_m(f,\theta) - J_0\left(\frac{2\pi f}{c} r_m \sin\theta\right) \right] \right|, \tag{3.10}$$

where $f \in [0.9, 8]$ kHz and $\theta \in [-60°, 60°]$. The evaluation of the maximal error in (3.10) for different numbers of discrete sensors shows that having 16 elements on each ring results in a $\sim 10^{-6}$ difference between the expected and the achieved beampattern.

3.3.2 Calculating the Attenuation Coefficients

The goal of the presented step is to determine the attenuation weights of the beamformer as the frequency increases. In this stage, all the rings are effective in the beamforming process, so that the weight given to each ring is equal to one. As frequency

increases, the outer rings are attenuated until eventually, only one ring contributes to the beamforming process. This gradual elimination process is similar to sampling a piston with a smaller radius for higher frequencies. As explained in Section 3.2, this approach keeps the value of fR constant, resulting in constant beamwidth.

To find the frequency range in which the desired beamwidth remains constant, let us define the lowest and highest frequencies f_{L} and f_{H} for which the beamwidth is attained for a given CRA. These frequency bounds are determined by two weight combinations: when all the rings are active, i.e., $H_m(f_{\mathrm{L}}) = 1 \; \forall m \in [1, M]$, the lower bound of the frequency range satisfies

$$\beta_{\mathrm{BW}} = \frac{1}{N} \sum_{m=1}^{M} \mathcal{R}_m \left(f_{\mathrm{L}}, \frac{\theta_{\mathrm{BW}}}{2} \right) . \tag{3.11}$$

When only the innermost ring is active, i.e., $H_1(f_{\mathrm{H}}) = 1$ and $H_m(f_{\mathrm{H}}) = 0$ for $m \neq 1$, the upper bound of the frequency range satisfies

$$\beta_{\mathrm{BW}} = \frac{1}{N_1} \mathcal{R}_1 \left(f_{\mathrm{H}}, \frac{\theta_{\mathrm{BW}}}{2} \right) . \tag{3.12}$$

To ensure that the beampattern is equal to 1 at boresight, we normalize it by the number of active sensors in the beamforming.

Since (3.11) and (3.12) are difficult to solve analytically, we use the bisection method to find the roots of the above equations in the range $f \in [0, 10]$ kHz. The bisection method yields $f_{\mathrm{L}} = 1617$ Hz and $f_{\mathrm{H}} = 9405$ Hz (we limit the maximal frequency to 8000 Hz). By repeating this process for all M possible array radii constellations (i.e., when all rings are active, the $M-1$ inner rings are active, etc.), we find the M transition frequencies where the outermost ring is fully attenuated. Given a frequency in the range $f \in [f_{\mathrm{L}}, f_{\mathrm{H}}]$, we can design the beamformer to achieve θ_{BW}, as described next.

We define f_m as the frequency obtaining the desired beamwidth in an m rings array (where $0 < m < M$). We denote the total number of sensors in an m rings CRA as $\hat{N}_m \triangleq \sum_{k=1}^{m} N_k$. Given a frequency in the transition band $f \in [f_{m+1}, f_m]$, the m inner rings are active and the $m+1$ ring is attenuated such that:

$$H_i(f) = \begin{cases} 1, & i \in [1, m] , \\ \in (0, 1) , & i = m+1. \end{cases} \tag{3.13}$$

To obtain the desired beamwidth, the exact weight value, applied on the outer $m+1$ ring, satisfies

$$\beta_{\mathrm{BW}} = \frac{\sum_{i=1}^{m} \mathcal{R}_i \left(f, \frac{\theta_{\mathrm{BW}}}{2} \right) + H_{m+1}(f) \, \mathcal{R}_{m+1} \left(f, \frac{\theta_{\mathrm{BW}}}{2} \right)}{\hat{N}_m + H_{m+1}(f) \, N_{m+1}} . \tag{3.14}$$

Some mathematical manipulations of (3.14) lead to the attenuation amplitude of the outer ring:

$$H_{m+1}(f) = \frac{\beta_{\mathrm{BW}}\hat{N}_m - \sum_{i=1}^{m} \mathcal{R}_i\left(f, \frac{\theta_{\mathrm{BW}}}{2}\right)}{\mathcal{R}_{m+1}\left(f, \frac{\theta_{\mathrm{BW}}}{2}\right) - \beta_{\mathrm{BW}} N_{m+1}}\,. \tag{3.15}$$

Hence, the weight value for the mth ring ($m \in [1, M]$) is given by

$$H_m(f) = \begin{cases} 1, & f < f_m, \\ \frac{\beta_{\mathrm{BW}}\hat{N}_{m-1} - \sum_{i=1}^{m-1} \mathcal{R}_i\left(f, \frac{\theta_{\mathrm{BW}}}{2}\right)}{\mathcal{R}_m\left(f, \frac{\theta_{\mathrm{BW}}}{2}\right) - \beta_{\mathrm{BW}} N_m}, & f_m < f < f_{m-1}, \\ 0, & f_{m-1} < f. \end{cases} \tag{3.16}$$

The array beampattern of the lowpass filters beamformer (designed according to (3.16)) and without them (i.e., the result of a simple summation) are shown in Figure 3.1. We see that in the frequency range $f > f_{\mathrm{L}}$, the mainlobe width after applying the filters (plot (b)) remains constant, as opposed to the changing beamwidth shown in Figure 3.1a. However, in the lower frequency range $f < f_{\mathrm{L}}$, the main lobe is wider as the frequency decreases in both cases. The next step of the suggested beamformer aims to extend the frequency range of the constant beamwidth. In the suggested approach, the array filters are designed as bandpass filters, instead of lowpass filters, by utilizing the circular geometry.

3.3.3 Weights Adaptation in Low Frequencies

We aim to extend the frequency range for which the beampattern attains the desired beamwidth. To do so, we examine the beampattern of a single ring constructed of discrete sensor elements. As mentioned in Section 2.3, the beampattern of the discrete ring is approximately equal to the continuous beampattern if a sufficient number of sensors is chosen. Hence, the beampattern of the discrete ring is similar to the zero-order Bessel function of the first kind, shown in (3.4).

In the first beamformer design step, we assumed that all the rings are active in low frequencies, resulting in lowpass filters applied on the CRA. As a result, the lowest frequency for which the desired beamwidth is attained depends on the piston beampattern shown in (3.1). However, the beampattern of a single ring allows an extension of the low-frequency range. By assuming that a single ring with radius r is active, we find that the beamwidth is satisfied if

$$\frac{2\pi f}{c} r \sin\left(\frac{\theta_{\mathrm{BW}}}{2}\right) \approx 1.41\,. \tag{3.17}$$

From (3.17), we note that at frequencies lower than f_{L}, the beampattern can attain

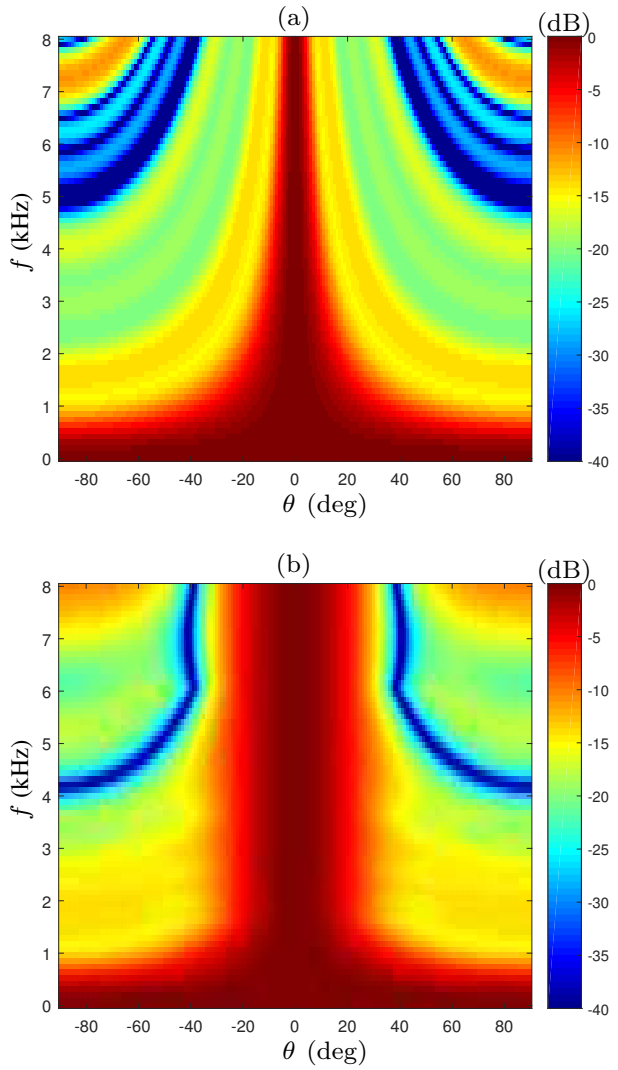

Figure 3.1: Beampatterns of the 6-ring CRA, (**a**) without constant-beamwidth beamformer weights, and (**b**) after applying the constant-beamwidth beamformer weights.

the desired beamwidth if we design the array to hold a single active ring. Therefore, we add the following step to the design process: At low frequencies, all the CRA weights are null except for the outer ring. As the frequency increases, we gradually add the inner rings while maintaining a constant beamwidth, until the frequency reaches the lower bound $f = f_{\mathrm{L}}$. From that point, where all the rings are active in the beamformer, we repeat the gradual elimination of the outer ring as described in the previous section. Having the extended beamwidth approach, the new lower frequency bound is given by

$$\beta_{\mathrm{BW}} = \frac{1}{N_M}\mathcal{R}_M\left(f_{\mathrm{L}}^{\mathrm{new}}, \frac{\theta_{\mathrm{BW}}}{2}\right). \tag{3.18}$$

Equation (3.18) is satisfied for $f_{\mathrm{L}}^{\mathrm{new}} = 940$ Hz, compared to the lower bound in the original implementation which was $f_{\mathrm{L}} = 1617$ Hz. By designing the filters as bandpass filters, we can extend the constant-beamwidth frequency range. To calculate

the weights for the inner rings in the extended range $f \in [f_{\mathrm{L}}^{\mathrm{new}}, f_{\mathrm{L}}]$, we repeat the bisection process and find the transition frequency bins.

In the suggested design, we denote f_m as the frequency where the $M-m$ outer rings are active in the beamformer and the mth inner ring is gradually enhanced. For $f \in [f_{m+1}, f_m]$, the weight of the outer ring is $H_i(f) = 1 \ \forall i \in [m+1, M]$ while the inner mth ring is added to the array such that $H_m \in (0,1)$. Since we aim to increase the constant-beamwidth frequency range, the weight given to the inner ring satisfies

$$\beta_{\mathrm{BW}} = \frac{\sum_{i=m+1}^{M} \mathcal{R}_i\left(f, \frac{\theta_{\mathrm{BW}}}{2}\right) + H_m(f)\, R_m\left(f, \frac{\theta_{\mathrm{BW}}}{2}\right)}{\tilde{N}_m + H_m(f)\, N_m}, \tag{3.19}$$

where $\tilde{N}_m = \sum_{k=m+1}^{M} N_k$ is the total number of sensors in the active outer rings. From (3.19), the weight given to the inner ring in the lower frequency range is

$$H_m(f) = \frac{\beta_{\mathrm{BW}} \tilde{N}_m - \sum_{i=m+1}^{M} \mathcal{R}_i\left(f, \frac{\theta_{\mathrm{BW}}}{2}\right)}{\mathcal{R}_m\left(f, \frac{\theta_{\mathrm{BW}}}{2}\right) - \beta_{\mathrm{BW}} N_m}. \tag{3.20}$$

The beampattern of the extended beamwidth CRA (EXT-CRA) compared to the unmodified CRA in the low-frequency range $f \in [0, 3000]$ Hz is shown in Figure 3.2. The gradual addition of the rings, starting from the outer ring inwards, provides better beamwidth consistency in frequencies smaller than f_{L}. For frequencies lower than 940 Hz (for which only the outer ring is active), we cannot modify the beampattern, so the beamwidth is wider as the frequency decreases.

3.3.4 Directivity Index Improvement

In Section 3.3.3, the beamformer filters were reshaped to broaden the frequency range that attains the desired beamwidth. We can, however, improve the beamformer's performance further by relaxing the beamwidth constraint at lower frequencies.

In the suggested step, the weights of the 2 outer rings are modified for frequencies $f \leq f_{\mathrm{L}}^{\mathrm{new}}$ to maximize the DI. The DI represents the array gain in a diffuse noise environment and is defined as [4]

$$\mathcal{D}\left[\underline{\boldsymbol{h}}(f)\right] \triangleq \frac{\left|\underline{\boldsymbol{h}}(f)^T\, \underline{\boldsymbol{d}}(f, \theta_0, \phi_0)\right|^2}{\underline{\boldsymbol{h}}(f)^T\, \boldsymbol{\Gamma}\, \underline{\boldsymbol{h}}(f)}, \tag{3.21}$$

where the pseudo-coherence matrix $\boldsymbol{\Gamma}$ is given by

$$\boldsymbol{\Gamma} \triangleq \frac{1}{4\pi} \int_0^{2\pi} \int_0^{\pi} \underline{\boldsymbol{d}}(f, \theta, \phi)\, \underline{\boldsymbol{d}}(f, \theta, \phi)^T \sin\theta d\theta d\phi. \tag{3.22}$$

To improve the DI in low frequencies, we search for the optimal ratio between the outermost ring and the second outermost ring weights under the constraint that the

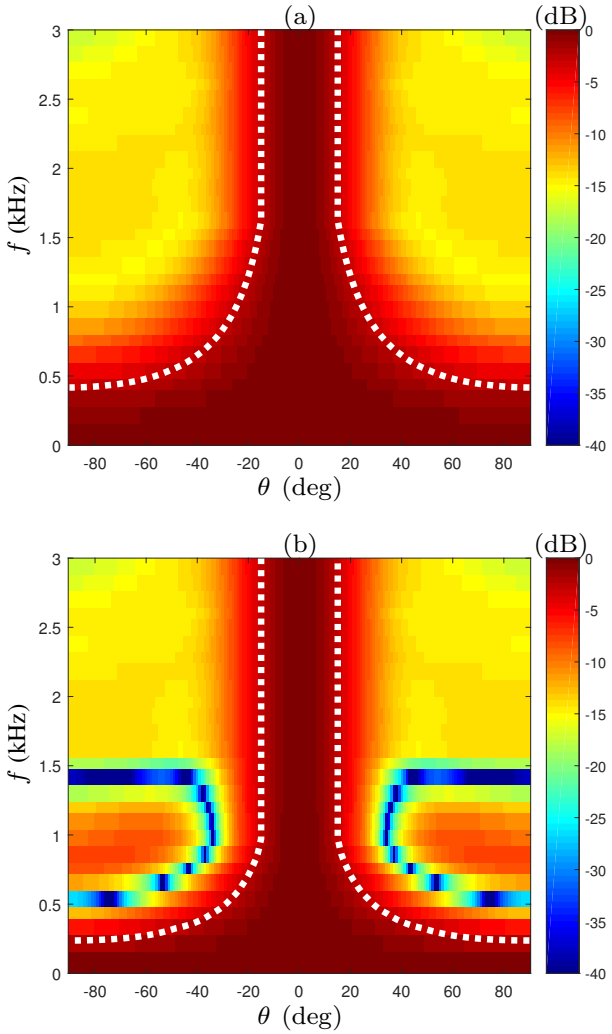

Figure 3.2: Beampatterns of the 6-ring CRA, (**a**) without lower frequencies beamwidth extension, and (**b**) with the extension. The dashed line marks the amplitude in which the BW is defined $\beta_{\mathrm{BW}} \triangleq -3$ dB.

beamwidth is wider than θ_{BW}. Hence, we can utilize the circular geometry in the lower frequency range to gain higher DI. A similar approach applied on one-dimensional ULA was suggested in [43]. The results of the proposed design compared to the previous stages are presented in Section 3.4.

3.3.5 Time Domain Filter Implementation

The previous sections presented the desired beamformer response given specified frequency characteristics. In this section, we determine the temporal FIR filter coefficients. The design aims to approximate the resulting beamformer response to the ideal beamformer described above.

The time-domain FIR filters are calculated from their frequency responses using the signal processing toolbox of MATLAB, which minimizes the integrated squared error

defined as [53]:

$$\epsilon_2 = \int_0^{\pi} W(\omega) \left(\hat{H}(\omega) - H(\omega) \right)^2 d\omega \,, \tag{3.23}$$

where ω is the normalized frequency, $W(\omega)$ is the non-negative weighting function, $\hat{H}(\omega)$ is the actual filter response and $H(\omega)$ is the ideal response. The FIR filters are designed to have the same number of coefficients to maintain a fixed delay. The number of coefficients is chosen based on the mainbeam constraint [54]. The constraint ensures that the resulting beampattern at θ_{BW} is approximately equal to β_{BW} over a grid of frequencies in the range $f_i \in [f_{\mathrm{L}}^{\mathrm{new}}, f_{\mathrm{H}}]$:

$$\epsilon_{\mathrm{BW}} = \sum_i \left| \mathcal{B}\left[\underline{\boldsymbol{h}}(f_i), \theta_{\mathrm{BW}} \right] - \beta_{\mathrm{BW}} \right|^2 \Delta f \,. \tag{3.24}$$

By iterating over a range of possible filter lengths, a 36-coefficient FIR filter per-ring was designed. This length compromises between the mainbeam constraint and the short delay requirement.

In addition, the beamformer should maintain a uniform gain over the whole frequency range to prevent distortion of the input signal. Hence, following the FIR filtering, the output results are summed and processed by an additional FIR normalization filter. The normalization filter taps are calculated by summing the absolute values of the previously calculated sensor filters and multiplied by the number of elements per ring, as described in [42].

The entire design process is summarized in Algorithm 3.1. Note that even though the results shown in this section are for $\theta_{\mathrm{BW}} = 30^{\circ}$, the proposed beamformer design supports significantly lower beamwidths. However, choosing a smaller beamwidth increases the minimal frequency for which the desired beamwidth is achieved as can be observed from (3.17). Moreover, a lower beamwidth may require more sensors on each ring, as obtained from (3.9).

The weights matrix of the suggested beamformer is shown in Figure 3.3a. The y-axis represents frequency bins used for designing the array filters, and the x-axis represents the ring index (1–6), where index 1 is the innermost ring. Notice the gradual addition of inner rings in the lower frequency range, followed by the elimination of outer rings as the frequency increases. The colorbar indicates the attenuation weight value, ranging from 0 to 1. The final beampattern of the suggested beamformer is presented in Figure 3.3b. The -3 dB amplitude is marked by the dashed white lines, which define the beamwidth. We note that there is a slight degradation in the beamwidth consistency compared to the ideal beampattern, yet overall, the desired beamwidth is attained over a wide range of frequencies.

Algorithm 3.1 Constant-Beamwidth CRA Beamformer Design

Calculate the attenuation weight:
for $m \in [1, M]$ **do**
find f_m by solving: $\beta_{\mathrm{BW}} = \frac{\sum_{i=1}^{m} \mathcal{R}_i\left(f_m, \frac{\theta_{\mathrm{BW}}}{2}\right)}{\sum_{i=1}^{m} N_i}$ using the Bisection algorithm.
end for
Define $f_{\mathrm{L}} = f_M$, $f_{\mathrm{H}} = \min(f_1, 8000)$.
for $f \in [f_{\mathrm{L}}, f_{\mathrm{H}}]$ **do**
Calculate ring weight based on (3.16).
end for
Modify the beamformer to expand the constant-beamwidth frequency range:
for $m \in [1, M]$ **do**
find f_m by solving: $\beta_{\mathrm{BW}} = \frac{\sum_{i=m}^{M} \mathcal{R}_i\left(f_m, \frac{\theta_{\mathrm{BW}}}{2}\right)}{\sum_{i=m}^{M} N_i}$ using the Bisection algorithm.
end for
Define $f_{\mathrm{L}}^{\mathrm{new}} = f_M$.
for $f \in [f_{\mathrm{L}}^{\mathrm{new}}, f_{\mathrm{L}}]$ **do**
Compute the ring weight based on (3.20).
end for
Improve the DI in lower frequencies:
for $f \in [0, f_{\mathrm{L}}^{\mathrm{new}}]$ **do**
let $H_M(f) = 1$, find $H_{M-1}(f)$ s.t $\underline{\boldsymbol{h}}(f)^T \boldsymbol{\Gamma} \underline{\boldsymbol{h}}(f)$ is minimal.
end for
Implement the desired filters in time domain.
Calculate the normalization factor for each frequency.

3.4 Performance Analysis

To evaluate the performance of the different beamformers discussed above, we use the DI and WNG measures. We also measure the first sidelobe level of the beampatterns and compare the beamwidth consistency throughout a range of frequencies and different beamwidths. These performance measures are used to compare the following beamformers:

1. Constant-beamwidth ULA, which is designed using the algorithm suggested in [42], based on the symmetry around the central element. The length of the ULA equals the diameter of the CRA, i.e., $L = 50$ cm. The element spacing is $d = 3.5$ cm to prevent spatial aliasing, and the ULA consists of 15 sensors;

2. A 6-ring CRA applied with the lowpass design (CRA-LP) (as described in Section 3.3.2);

3. A 6-ring CRA with the lower frequency beamwidth extension (EXT-CRA), suggested in Section 3.3.3;

4. The improved DI beamformer (EXT-CRA-I) in low frequencies by allowing a moderate widening of the beampattern, as described in Section 3.3.4

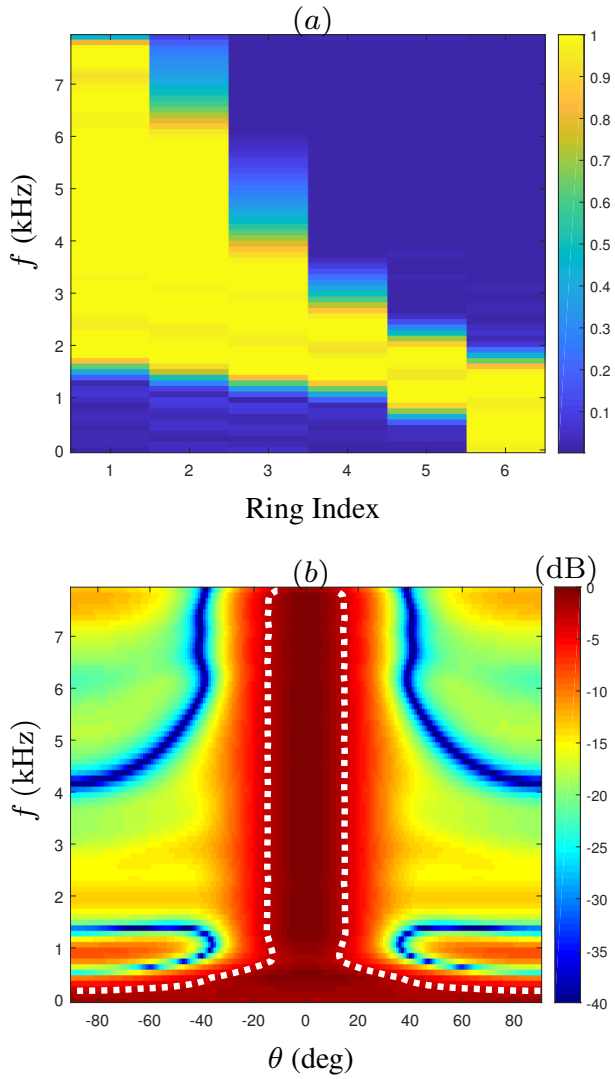

Figure 3.3: Constant-beamwidth beamformer for 6-ring CRA implemented with temporal FIR filters. (**a**) Weight values applied on the rings; (**b**) beampattern.

All the performance measures presented in the following section were calculated after implementing each beamformer in the time domain, as described in Section 3.3.5. Note that even though the number of sensor elements in the CRA is larger compared to the ULA, the suggested CRA beamformer is composed of only 6 channels (equivalent to the number of rings in the array). Moreover, the beamformer is designed to attain constant elevation beamwidth with efficient application in a physical setup. As a result, the existing UCCA beamformers (mentioned in the introduction) which require considerably more physical equipment and computational resources are not presented in this section.

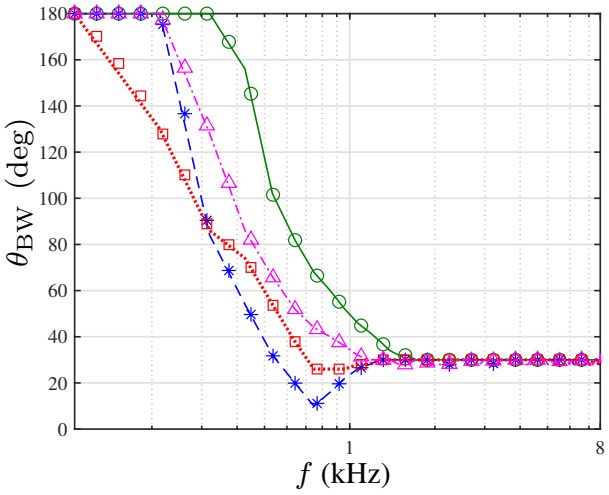

Figure 3.4: Beamwidth θ_{BW} as a function of frequency for different beamformers: CRA-LP (solid line with circle), EXT-CRA (dashed line with asterisks), EXT-CRA-I (dotted line with squares), and ULA (dash-dotted line with triangles).

3.4.1 Beamwidth Consistency

The main objective of the proposed beamformer is to design a constant-beamwidth beampattern over a wide range of frequencies. Figure 3.4 presents the beamwidth of each beamformer as a function of frequency. Compared to the CRA-LP design, the adaptation of the weights in lower frequency (EXT-CRA) results in smaller beamwidth in the frequencies $f \in [940, 1617]$ Hz. Furthermore, for frequencies lower than 940 Hz, the beamwidth increases as the frequency decreases for all the examined beamformers. However, the beamwidth after the suggested modification is smaller compared to CRA-LP and the ULA. In addition, we note that the DI improvement in the EXT-CRA-I beamformer affects the attained beamwidth compared to the EXT-CRA. Due to the time domain implementation, there is an inconsistency of the beamwidth in lower frequencies for the EXT-CRA beamformer. The EXT-CRA-I incorporates an additional ring in the beamforming process, which smoothes the ideal frequency response at lower frequencies. Hence, the frequency responses of the FIR filters are closer to the desired responses, which improves the beamwidth consistency in the lower frequency range.

3.4.2 Directivity Index and White Noise Gain

The WNG is a measure of the array gain in a spatially uncorrelated noise environment, which is a good indicator of the performance robustness to sensor imperfections. The WNG is calculated as [4]

$$\mathcal{W}\left[\underline{\boldsymbol{h}}\left(f\right)\right]) = \frac{\left|\underline{\boldsymbol{h}}(f)^T \underline{\boldsymbol{d}}(f, \theta_0, \phi_0)\right|^2}{\underline{\boldsymbol{h}}(f)^T \underline{\boldsymbol{h}}\left(f\right)}. \tag{3.25}$$

Figure 3.5 shows the performances of the discussed beamformers in terms of DI and

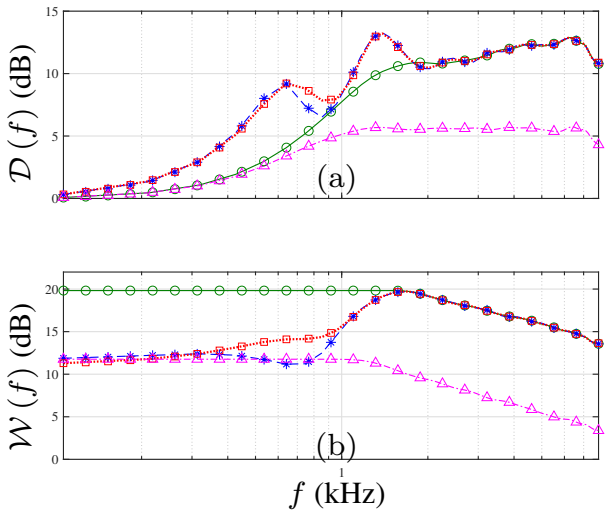

Figure 3.5: Performance measures for CRA-LP (solid line with circle), EXT-CRA (dashed line with asterisks), EXT-CRA-I (dotted line with squares), and ULA (dash-dotted line with triangles): (**a**) DI, and (**b**) WNG, as a function of frequency.

WNG. Notice that the CRA geometry achieves higher DI compared to the ULA. In the frequency range $f > 1620$ Hz, the average difference is 7 dB. Note the improvement in terms of DI between CRA-LP and the EXT-CRA beamformer in the lower frequency range. Furthermore, the EXT-CRA-I design achieves higher DI around $f = 846$ Hz compared to EXT-CRA, as desired.

The WNG comparison in Figure 3.5b shows that the WNG of the CRA is 10 dB higher than the ULA for frequencies in the range $f > 1620$ Hz. Since the number of sensors in the LP-CRA is significantly higher than the number used in the ULA, it is more robust to incoherent noise due to electronic noise and errors in the sensor placing. Moreover, despite the improvements in beamwidth consistency, the WNG was smaller than the WNG achieved with the non-modified CRA beamformer. For frequencies $f < f_{\mathrm{L}}$, there is a 8 dB difference between the CRA-LP beamformer and the EXT-CRA beamformer.

3.4.3 Sidelobe Attenuation

The sidelobe attenuation can be helpful in attenuating signals from out-of-beamwidth directions and improving the directivity index. Figure 3.6 shows the beampatterns of the EXT-CRA-I and ULA beamformers calculated at different frequencies in the range $f \in [2000, 8000]$ Hz. In terms of sidelobe attenuation, we see that the first sidelobe of the EXT-CRA-I beamformer is lower than the sidelobe of the ULA by 7 dB. The primary reason for the better side-lobe attenuation performance in the proposed algorithm is the explicit calculation of the beampattern beamwidth for every frequency bin, with attenuation of outer rings. Thus, most of the beampattern power is concentrated within the mainbeam and the leakage to the sidelobes is minimized. Furthermore,

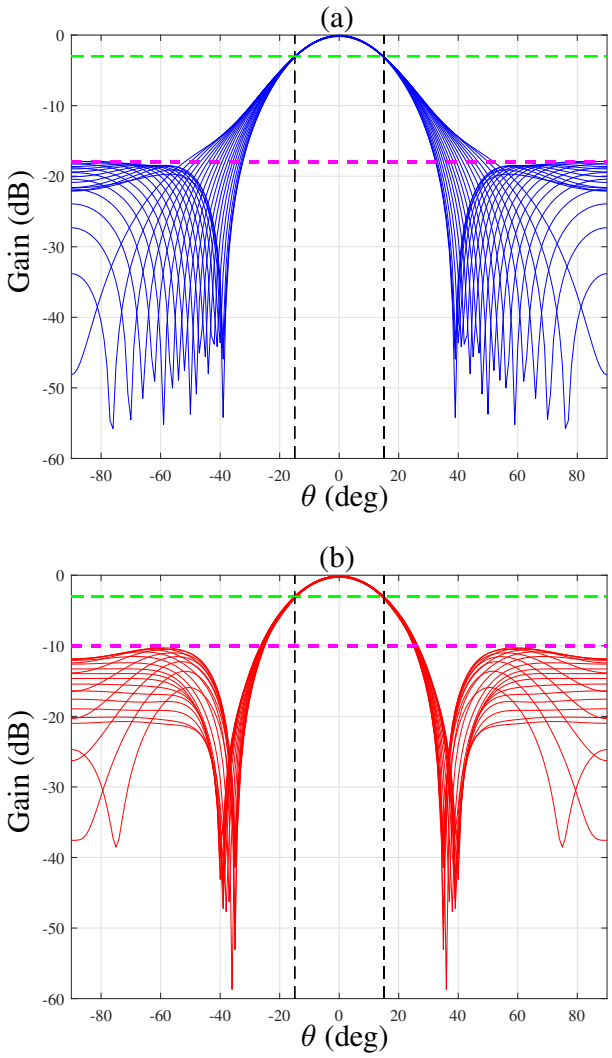

Figure 3.6: Beampatterns at different frequencies calculated for (**a**) EXT-CRA-I, and (**b**) ULA. The first sidelobe level, the desired BW and the -3 dB amplitude are marked by a dash-point line, solid line and dotted line, respectively.

we observe that both arrays satisfy the beamwidth constraint. By utilizing the post-normalization filter a uniform gain beampattern is achieved over the entire frequency range, as desired.

3.4.4 Beamwidth Variability

An important characteristic of a constant-beamwidth beamformer is its ability to support variable system specifications. Thus, in this section, we present the beamformers' performance for different desired beamwidths. That is, the beamformers' competence to attain various beamwidths (under a constant ring constellation and number of sensors) is examined. Figure 3.7 shows beampatterns for $\theta_{\text{BW}} = [20°, 30°, 40°, 50°]$ of the EXT-CRA beamformer. Note that under a similar geometry, the proposed beamformer attains multiple specified beamwidths. Marked by dashed lines, the beamwidth remains

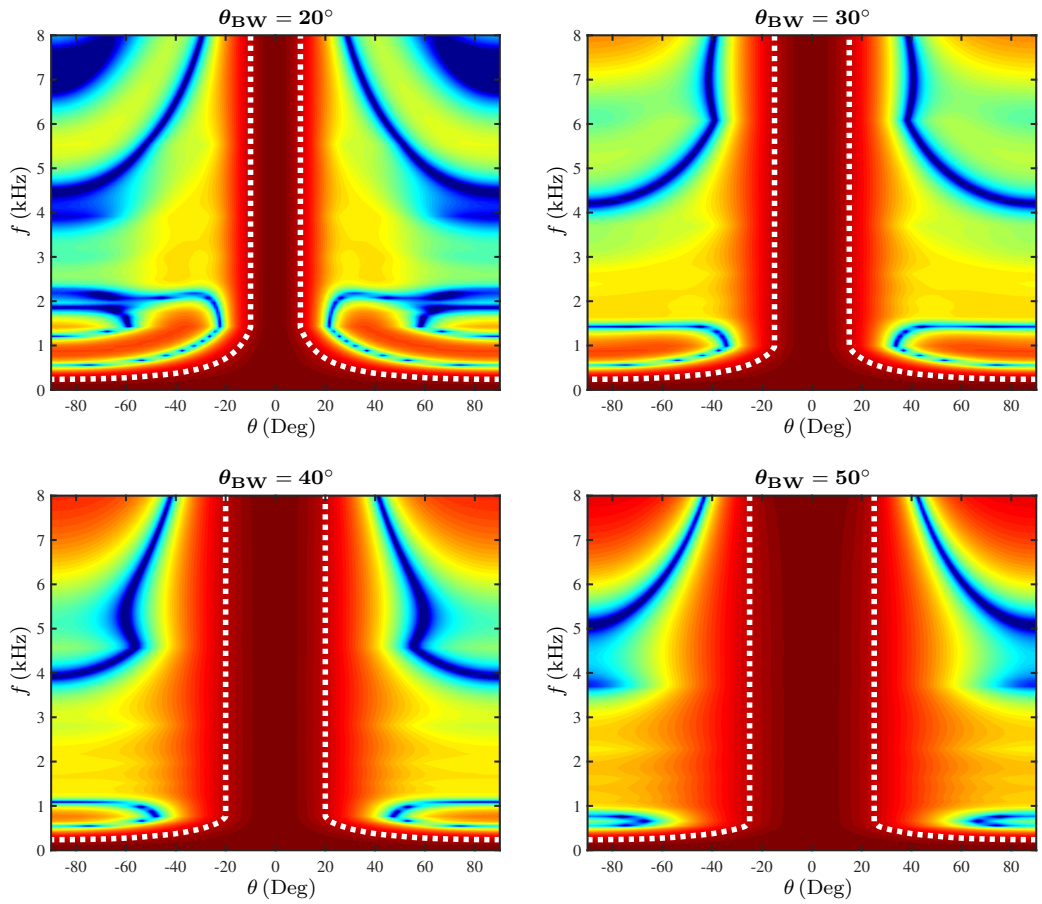

Figure 3.7: Beampatterns of a 6-ring CRA with several desired beamwidth specifications. The presented beampatterns are for $\theta_{\mathrm{BW}} = [20°, 30°, 40°, 50°]$, ordered from left to right.

consistent throughout a wide range of frequencies. As the required beamwidth is wider, the minimum frequency for which it is attained decreases. The relation between the lower bound frequency and the beamwidth was shown in (3.17). At lower frequencies, only the outermost ring is active while the rest of the rings are fully attenuated. Consequently, the radius is constant and the lower frequency bound is inversely dependent on the desired beamwidth.

Moreover, as the beamwidth is wider, the sidelobe levels are higher in high frequencies ($f > 6$ kHz). The attenuation of outer rings occurs in lower frequencies for wider beamwidths. As a result, as the frequency increases, the significant weight is applied to the innermost ring. Since the ring beampattern shares the characteristics of the zero-order Bessel function, the first sidelobe is closer as the frequency increases. Hence, as the inner ring is more dominant for a given wider beamwidth, the sidelobes are emphasized in higher frequencies.

The beamwidth and the sidelobe level affect the beamformers' performance. The DI and WNG for the different beamwidths are presented in Figure 3.8. As expected, the DI

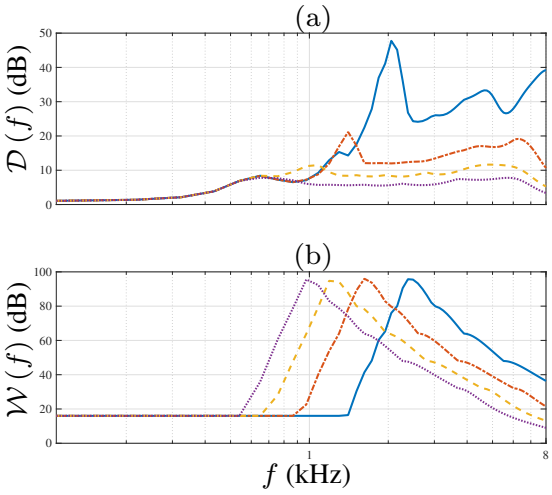

Figure 3.8: (**a**) DI, and (**b**) WNG, as a function of frequency, for EXT-CRA with beamwidths: $\theta_{\mathrm{BW}} = 20°$ (solid line), $\theta_{\mathrm{BW}} = 30°$ (point-dashed line), $\theta_{\mathrm{BW}} = 40°$ (dashed line) and $\theta_{\mathrm{BW}} = 50°$ (dotted line).

increases as the beamwidth is narrower. Note that the maximal DI for each beamwidth is obtained at lower frequencies for wider beamwidths. In addition, the decrease of the DI in higher frequencies is shown for $\theta_{\mathrm{BW}} = [30°, 40°, 50°]$. The degradation is caused due to the sidelobe levels, as discussed above.

By examining the WNG plot, we note that as the beamwidth is wider, the increase and the following decrease of the WNG occurs at smaller frequencies. Since the beamwidth is achieved at lower frequencies, the gradual addition of inner rings increases the WNG. When all the rings in the CRA are active, the attenuation of the outer rings gradually reduces the WNG. As the number of sensors is equal per ring, the WNG graphs present an equivalent trend with shifting along the frequency axis.

3.5 Summary

We have introduced beamformers for concentric ring arrays, designed to have a constant beamwidth over a wide range of frequencies. The suggested beamformers are designed to be incorporated in a multi-beam system of circular ceiling arrays. We described the advantages of the discussed system and the specifications required from the beamformer. The proposed design applies the same filter to all the elements on each ring. This constraint lowers computational complexity in design and enables a physical setup that requires fewer resources. In addition, we modified the lower frequency band by reducing the number of active rings in that range. The suggested modification utilizes the geometrical properties of the array to extend the frequency range for which a constant beamwidth is achieved. We also added an improved directivity index design in frequencies lower than the range limits and implemented the beamformer in the time domain with FIR filters. The proposed beamformer showed superior performance in

terms of directivity index, white noise gain, beamwidth consistency and sidelobe attenuation, compared to a constant-beamwidth beamformer of the same order, designed for a ULA.

Chapter 4

Constant-Beamwidth Nonuniform CRAs

This chapter introduces improved directivity factor beamformers, with constant beamwidth. Unlike the method proposed in Chapter 3, the presented methodology discusses nonuniformly spaced rings arrays. Moreover, the beamformers' weights are determined by solving an optimization problem (rather than a pre-defined window function). The principal concept of the suggested beamformer is presented in Section 4.1. In Section 4.2, the optimization constraints, the cost function, and the design algorithm are introduced. The performance of the suggested beamformers is evaluated in Section 4.3, following with conclusions drawn in Section 4.4.

4.1 Background

In the previous chapter, we have presented a window-based beamformer, applied to a uniformly spaced CRA. In this chapter, we discuss two constant-beamwidth beamformers, with different degrees of freedom. In the proposed designs, the rings' positions are selected by solving an optimization problem. Thus, the resulting CRA constellation is not restricted to be uniformly spaced. In addition to the constant beamwidth constraint, the proposed methods aim to maximize the array directivity factor. Hence, we introduce constant beamwidth beamformers with improved DF, designed for CRA geometry. First, we define a quadric programming optimization problem [49], aiming to maximize the DF while maintaining a constant beamwidth on a set of linearly spaced UCCA. Since the geometry is set, we perform the optimization on each frequency bin individually. Following, we propose a constant beamwidth beamformer with no predefined radii locations. To achieve the maximal DF while maintaining the specified beamwidth, we propose a methodology to simultaneously choose the optimal ring locations and design the beamformer weights. The number of rings in the array is specified before performing the optimization. The optimal solution is chosen from a rigid grid of possible radii and performed coherently over all the frequency bins. To

ensure equal or better DF compared to the incoherent beamformer, the DF of the incoherent beamformer is incorporated in the nonuniform beamformer cost function.

As mentioned in Section 2.2, the suggested beamformers utilize the CRA geometry. That is, in all of the suggested beamformers the microphones in each ring share joint weights. Each ring in the CRA is constructed from equally spaced omnidirectional microphones. To avoid spatial aliasing the inter-sensor distance δ should be smaller than half the minimal wavelength $\lambda_{\min}$ [51], meaning that $\delta \leq \lambda_{\min}/2$. Consequently, the inner spacing on each ring should satisfy

$$\delta_m = 2r_m \sin\left(\frac{\pi}{N_m}\right) \approx \frac{2\pi r_m}{N_m} \leq \frac{\mathrm{c}}{2f_m^{\max}}\,, \tag{4.1}$$

where δ_m denotes the inner spacing between two adjacent microphones on the m^{th} ring. The highest frequency in which the m^{th} ring is effective in the beamforming process is marked by $f_m^{\max}$. Thus, in frequencies in the range where $f_m^{\max} < f$ the m^{th} ring is completely attenuated. From (4.1), the number of equally spaced elements in ring m is given by

$$N_m = \left\lceil \frac{4\pi r_m f_m^{\max}}{\mathrm{c}} \right\rceil. \tag{4.2}$$

Since the number of microphones in each ring should be an integer, the value in (4.2) is rounded up.

The DF is is an important characteristic of any beamformer [52]. Hence, one of the main goals of the beamformers proposed is to maximize the DF of the CRAs. The DF denotes the relative power between the beampattern in the direction-of-interest $(\theta_{\mathrm{d}}, \phi_{\mathrm{d}})$ with respect to the entire 3-D beampattern. The DF can be interpreted as the beamformer ability to suppress spatial noise from directions other than the look direction. While the DF is an important measure of the beamformer performance (especially in 3-D broadband applications), most of the existing works on designing UCCA beamformers do not consider the DF as an optimization parameter. In the following sections, the beamforming algorithms include DF optimization, and the results are presented in Section 4.3. For simplicity, all the results shown in this chapter regard the direction-of-interest as the boresight direction of the CRA.

4.2 Array Pattern Synthesis

In this section, a nonuniform constant beamwidth beamformer is suggested. The CRA has no pre-arranged ring locations, which are selected dynamically in the design process. The beamformer weights are designed by solving a quadratic programming optimization problem. The objective of the optimization problem is to maximize the DF under a set of constraints to ensure constant beamwidth. The user-defined parameters are the desired beamwidth and the number of rings in the CRA. Ultimately, the sparse problem

solution selects a set of ring locations out of a rigid grid of possible radii. Since the ring locations should be consistent for all frequencies, the optimization is performed over the entire frequency band. In this section, an additional beamformer is presented. This design is proposed for uniformly spaced CRAs, solving an equivalent optimization problem on a pre-defined set of rings. The solution of the uniform beamformer is then utilized in the nonuniform beamformer to attain superior performance.

The following section describes several components in the beamformer design: First, the problem constraints are presented in Section 4.2.1. The optimization constraints are defined to attain constant beamwidth over a wide band of frequencies while selecting a subset of rings out of a radii grid. Next, Section 4.2.2 discusses the optimization cost function. The cost function is constructed of weighted summation of the DF over different frequencies. The frequencies are weighted based on the result of an additional optimization problem, designed for uniformly spaced CRA. Hence, we present the uniform CRA beamformer and the weighting method. The uniform beamformer performance will be shown in Section 4.3 in comparison with the nonuniform beamformer. Finally, the time-domain implementation of the ideal beamformer is suggested in Section 4.2.3.

We denote the uniformly discretized frequency space as $\{f_j\}_{j=1}^{J} \in \Omega$, containing J frequency bins. Out of a high-resolution grid of possible ring positions, a set of ring positions is selected by solving an optimization problem. The grid from which the ring locations are chosen is denoted by $\underline{\boldsymbol{r}} = [r_1, r_2, ..., r_{N_\mathrm{R}}]$. The grid vector contains N_R radii, indicating the number of optional ring radii in the grid. By setting the number of desired rings in the optimized array to M, the objective of the optimization problem is to find a set of M radii out of the possible N_R radii. Therefore, $\forall f_j \ \{f_j\}_{j=1}^{J} \in \Omega$ the weights vector applied on the array satisfies:

$$\underline{\boldsymbol{h}}\left(f_j\right) = \begin{cases} \{H_k\left(f_j\right)\}_{k\in\mathcal{K}}, & \text{for selected rings} \\ 0, & \text{otherwise,} \end{cases} \tag{4.3}$$

where $\mathcal{K}$ is the set of M chosen indices i.e. $\mathcal{K} \subseteq [1, N_\mathrm{R}]$. The chosen indices should be identical over the entire frequency space Ω.

4.2.1 Optimization Constraints

The beamformer is designed to have frequency-invariant characteristics by incorporating several constraints on the beampattern. First, to ensure that rings selected between different frequencies are all the same, a binary mask variable is introduced $\boldsymbol{\mathcal{M}}$. Each column of $\boldsymbol{\mathcal{M}}$, constructed of nulls and ones, indicates the selected radii at the corresponding frequency bin. Accordingly, the binary mask is of size $N_\mathrm{R} \times J$. Similarly, we define the weight matrix applied on the array as $\boldsymbol{\mathcal{H}}$. The array weight matrix is constructed from the CRA weights vectors over the entire frequency range, as shown

in (2.13):

$$\boldsymbol{\mathcal{H}} = \left[\underline{\boldsymbol{h}}\left(f_1\right) \quad \underline{\boldsymbol{h}}\left(f_2\right) \quad \cdots \quad \underline{\boldsymbol{h}}\left(f_J\right)\right] . \tag{4.4}$$

The binary mask is used to enforce the selected radii on the beamformer weight matrix. The correlation is achieved by the following constraint:

$$\mathcal{C}_1 \ : \ \mathbf{0} \leq \boldsymbol{\mathcal{H}} \leq \boldsymbol{\mathcal{M}} \, , \tag{4.5}$$

where $\mathbf{0}$ is the zero matrix of size $N_{\mathrm{R}} \times J$. Constraint (4.5) enforces the beamformer weights to be different from null only for the selected rings. That is, for each matrix element in indices (k, j) we get

$$\boldsymbol{\mathcal{H}}_{(k,j)} = \begin{cases} H_k\left(f_j\right), & \text{if } \boldsymbol{\mathcal{M}}_{(k,j)} = 1 \\ 0, & \text{if } \boldsymbol{\mathcal{M}}_{(k,j)} = 0, \end{cases} \tag{4.6}$$

where $0 \leq H_k\left(f_j\right) \leq 1$ (avoiding negative amplification values).

An additional constraint is required to guarantee that the number of rings is equal to M. When this constraint is enforced,

$$\mathcal{C}_2 \ : \ \boldsymbol{\mathcal{M}}^T \underline{\mathbf{1}}_{N_{\mathrm{R}} \times 1} = M \cdot \underline{\mathbf{1}}_{N_{\mathrm{R}} \times 1} \, , \tag{4.7}$$

each column of $\boldsymbol{\mathcal{M}}$ is compelled to include exactly M values different than 0. However, $\mathcal{C}_2$ does not secure that the selected rings between different frequency bins are identically located. A dependency between frequencies can be established by requiring that

$$\mathcal{C}_3 \ : \ \forall j \in [1, J-1] \ \ \left\| \boldsymbol{\mathcal{M}}_j - \boldsymbol{\mathcal{M}}_{j+1} \right\|_2^2 = 0 \, , \tag{4.8}$$

where $\| \cdot \|_2$ is the ℓ_2-norm and $\boldsymbol{\mathcal{M}}_j$ is the j^{th} column of the binary mask. A correspondence is formed between adjacent frequency bins using constraint $\mathcal{C}_3$. The binary mask must have every adjacent column identical to obtain $\mathcal{C}_3$. So, the optimization problem ensures that rings are consistently selected across the entire frequency range. Note that Constraint (4.8) is defined in a quadric form to maintain the convexity of the optimization problem.

Next, a constraint to avoid distortion of the signal of interest is introduced. The distortionless response constraint is given by

$$\mathcal{C}_4 \ : \ \forall \{f_j\}_{j=1}^{J} \in \Omega \quad \boldsymbol{\mathcal{H}}_j^T \underline{\boldsymbol{\mathcal{R}}}\left(f_j, \theta_{\mathrm{d}}\right) = 1 \, , \tag{4.9}$$

where $\underline{\boldsymbol{\mathcal{R}}}\left(f, \theta\right)$ denotes the ring responses vector, constructed from the response beampattern of each ring in the grid (defined in (2.16)). The j^{th} column of the weight matrix is denoted by $\boldsymbol{\mathcal{H}}_j$ (meaning the filter applied on the array at frequency f_j). Under constraint $\mathcal{C}_4$, the beampattern is equal to 1 at the direction of arrival.

Additionally, the design of the beamformer aims to maintain a constant beamwidth across a large frequency range. Accordingly, we denote a range of angles of interest by Θ, i.e., the elevation angles enclosed within the main beam $\left[0, \frac{\theta_{\mathrm{BW}}}{2}\right] \in \Theta$. We define the concatenated beampattern power vector at an elevation angle θ_i over a set of frequencies as

$$\underline{\boldsymbol{\mathcal{B}}}(\theta_i) = \begin{bmatrix} \boldsymbol{\mathcal{H}}_1^T \underline{\boldsymbol{\mathcal{R}}}(f_1, \theta_i) \\ \boldsymbol{\mathcal{H}}_2^T \underline{\boldsymbol{\mathcal{R}}}(f_2, \theta_i) \\ \vdots \\ \boldsymbol{\mathcal{H}}_J^T \underline{\boldsymbol{\mathcal{R}}}(f_J, \theta_i) \end{bmatrix}, \tag{4.10}$$

and denote a set of linear constraints for elevation angles within the mainbeam:

$$\mathcal{C}_5 \ : \ \forall \theta_i \in \Theta \ \ \underline{\boldsymbol{\mathcal{B}}}(\theta_i) \geq \beta_{\mathrm{BW}} \cdot \underline{\mathbf{1}}_{J \times 1}, \tag{4.11}$$

where β_{BW} marks the -3 dB amplitude. Hence, the beampattern magnitude within the mainbeam should be greater or equal to the magnitude value at the desired beamwidth. It should be noted that the CRA is constructed from a sufficient number of microphones on each ring, as discussed in Section 4.1. As a result, the array is independent of the azimuth angle ϕ. Therefore, we choose an arbitrary value of ϕ during the optimization process.

4.2.2 Directivity Factor Maximization

The constraints presented in Section 4.2.1 form a constant beamwidth beamformer with a distortionless response. Under the specified constraints, a set of M rings is chosen from a grid of possible places. As our objective is to maximize the DF under the distortionless response constraint in (4.9), the cost function can be defined as the sum of all the DF denominators within the frequency range:

$$\min_{\boldsymbol{\mathcal{H}}, \boldsymbol{\mathcal{M}}} \sum_{j=1}^{J} \boldsymbol{\mathcal{H}}_j^T \boldsymbol{\Gamma}(f_j) \boldsymbol{\mathcal{H}}_j . \tag{4.12}$$

The arguments in the summation are all non-negative. Therefore, the algorithm seeks to determine the optimal constellation of rings to minimize the overall summation result. Note, however, that the optimization is performed not only on the beamformer weights but also on the locations of the rings. In theory, a reduced-degrees-of-freedom optimization may outperform the sparse optimization presented above. If there is a known ring spacing, the optimization can be solved incoherently per frequency bin, which may result in a greater DF in certain frequencies. We suggest a weighted cost function to improve the performance of the nonuniform beamformer. The weighting coefficients would incorporate the results of an incoherent optimization (conducted on a set of uniform rings), as we will demonstrate next.

Incoherent Optimization of Uniform CRA

In this section, we consider an optimization problem involving equally-spaced rings. In the uniform scenario, the number of rings and their locations are pre-selected. The solution of the beamformer will be used as a weighting value for the nonuniform beamformer. The uniform beamformer weights are calculated by solving an optimization problem using quadratic programming, defined to optimize the DF in each frequency bin (given determined ring placements). The problem constraints in Section 4.2.1 are modified to allow solving each frequency bin independently, as follows: For each frequency, f_j, the distortionless constraint is given by

$$\mathcal{C}_1 \ : \ \underline{\boldsymbol{h}}^T(f_j)\,\underline{\boldsymbol{d}}(f_j,\theta_{\mathrm{d}},\phi_{\mathrm{d}}) = 1\,. \tag{4.13}$$

Under this constraint, the DF is maximized by

$$\min_{\underline{\boldsymbol{h}}(f_j)} \quad \underline{\boldsymbol{h}}^T(f_j)\,\boldsymbol{\Gamma}(f_j)\,\underline{\boldsymbol{h}}^T(f_j)\ . \tag{4.14}$$

The desired beamwidth is obtained by requiring

$$\mathcal{C}_2 \ : \ \forall\theta_i \in \Theta \quad \underline{\boldsymbol{h}}^T(f_j)\,\underline{\boldsymbol{d}}(f_j,\theta_i,\phi) \geq \beta_{\mathrm{BW}}\,. \tag{4.15}$$

Furthermore, to avoid negative amplification values, a third constraint on the weights amplitude is added:

$$\mathcal{C}_3 \ : \ \forall H_m(f_j) \in \underline{\boldsymbol{h}}(f_j) \quad 0 \leq H_m(f_j) \leq 1\,. \tag{4.16}$$

To sum up, given a frequency f_j the uniform constant beamwidth beamformer weights are calculated by:

$$\begin{aligned} \min_{\underline{\boldsymbol{h}}(f_j)} \quad & \underline{\boldsymbol{h}}^T(f_j)\,\boldsymbol{\Gamma}(f_j)\,\underline{\boldsymbol{h}}^T(f_j) \\ \text{s.t.} \quad & \underline{\boldsymbol{h}}^T(f_j)\,\underline{\boldsymbol{d}}(f_j,\theta_{\mathrm{d}},\phi_{\mathrm{d}}) = 1 \\ & \underline{\boldsymbol{h}}^T(f_j)\,\underline{\boldsymbol{d}}(f_j,\theta_i,\phi) \geq \beta_{\mathrm{BW}} \quad \forall\theta_i \in \Theta \\ & 0 \leq H_m(f_j) \leq 1 \quad \forall H_m(f_j) \in \underline{\boldsymbol{h}}(f_j)\,. \end{aligned} \tag{4.17}$$

The uniform beamformer is designed by solving (4.17). Following, the DF of the uniform beamformer is calculated at each frequency according to (2.17). We define the uniform beamformer DF vector as $\underline{\boldsymbol{\mathcal{D}}}_{\mathrm{u}} = [\mathcal{D}_{\mathrm{u}}(f_1), \mathcal{D}_{\mathrm{u}}(f_2), \cdots, \mathcal{D}_{\mathrm{u}}(f_J)]$, where $\mathcal{D}_{\mathrm{u}}(f_j)$ is the DF value of the uniform beamformer at frequency f_j. Next, the uniform beamformer DF will be incorporated in the nonuniform beamformer to yield superior performance of the nonuniform CRA.

Cost Function Modification

To outperform the uniform beamformer, $\underline{\boldsymbol{\mathcal{D}}}_{\mathrm{u}}$ is used as a weighting coefficient for the nonuniform beamformer cost function as:

$$\min_{\boldsymbol{\mathcal{H}},\boldsymbol{\mathcal{M}}} \sum_{j=1}^{J} \mathcal{D}_{\mathrm{u}}\left(f_j\right) \boldsymbol{\mathcal{H}}_j^T \boldsymbol{\Gamma}\left(f_j\right) \boldsymbol{\mathcal{H}}_j \,. \tag{4.18}$$

The weight value in frequency bins in which the uniform beamformer demonstrates a high DF value will be higher. Since the cost function aims to minimize the summation overall, the nonuniform beamformer will be impacted more by high-weighted frequency bins. Therefore, high weighted frequencies would affect the DF denominator and minimize its value. As a result, in frequency bins with higher weight values, the nonuniform beamformer would result with equivalently high DF. Hence, compared to the uniform beamformer, the nonuniform beamformer would produce a similar or better performance.

The sparse constant-beamwidth beamformer can be derived by solving the optimization problem:

$$\begin{aligned}
&\min_{\boldsymbol{\mathcal{H}},\boldsymbol{\mathcal{M}}} \sum_{j=1}^{J} \mathcal{D}_{\mathrm{u}}\left(f_j\right) \boldsymbol{\mathcal{H}}_j^T \boldsymbol{\Gamma}\left(f_j\right) \boldsymbol{\mathcal{H}}_j \\
\text{s.t.}\quad & \mathbf{0} \leq \boldsymbol{\mathcal{H}} \leq \boldsymbol{\mathcal{M}} \\
& \boldsymbol{\mathcal{M}}^T \underline{\mathbf{1}}_{N_{\mathrm{R}}\times 1} = M \cdot \underline{\mathbf{1}}_{N_{\mathrm{R}}\times 1} \\
& \|\boldsymbol{\mathcal{M}}_j - \boldsymbol{\mathcal{M}}_{j+1}\|_2^2 = 0 \quad \forall j \in [1, J-1] \\
& \boldsymbol{\mathcal{H}}_j^T \underline{\boldsymbol{\mathcal{R}}}\left(f_j, \theta_{\mathrm{d}}\right) = 1 \quad \forall \{f_j\}_{j=1}^{J} \in \Omega \\
& \underline{\boldsymbol{\mathcal{B}}}\left(\theta_i\right) \geq \beta_{\mathrm{BW}} \cdot \underline{\mathbf{1}}_{J\times 1} \quad \forall \theta_i \in \Theta \,.
\end{aligned} \tag{4.19}$$

4.2.3 Time Domain Filter Implementation

In a physical setup, the beamformer filters are implemented through temporal finite impulse response (FIR) filters. In the previous section, the weight matrix described the ideal beamformer given the problem constraints. In this section, we approximate the ideal beamformer by using FIR filters implemented in the time domain.

To achieve an accurate beamformer response with a sufficient number of filter taps, the ideal filters should be continuous. Therefore, an additional pre-processing step is added to the beamformer design: After solving (4.19), we examine the resulting weight matrix. For each ring (chosen by the optimized solution) an effective frequency band is determined. That is, we determine the frequency range in which each ring participates in the beamforming process (attenuated with a weight value above 0). In the following step, the incoherent optimization as in (4.17) is repeated. However, this time the optimization is performed on the set of non-uniformly spaced rings that participate in each frequency. This step yields an improved weights matrix, with smoothed filters per

Algorithm 4.1 Nonuniform Constant Beamwidth CRA

Initialization: set the desired number of rings in the array M, the discretized frequency space Ω and the elevation angle range Θ.
Weighting Coefficients Calculation:
define a uniformly spaced CRA with M rings.
for $f = f_j \quad \forall f_j \in \Omega$ **do**
  solve (4.17).
  update $\underline{\boldsymbol{\mathcal{D}}}_{\mathrm{u}}$ at f_j.
end for
Design the Sparse Nonuniform Beamformer:
define the radii grid $\underline{\boldsymbol{r}}$.
solve (4.19).
Smooth the Weight Matrix:
for $f = f_j \quad \forall f_j \in \Omega$ **do**
  define the effective rings in the CRA.
  solve (4.17) on the nonuniform geometry.
end for
Implement the Desired Filters in Time Domain.

ring.

The suggested pre-processing step has two significant advantages. First, the desired filters responses are modified to continuous forms. Having a smooth frequency response requires fewer FIR coefficients to achieve an approximate response of the ideal characteristics. Thus, in the perspective of a physical setup, the designed beamformer requires fewer resources, maintenance and is lower in cost. Second, having a restricting effective frequency range for each ring enables the use of fewer microphones per ring. Note that in (4.2) the number of microphone elements on each ring is determined by the maximal frequency in which the ring is effective. Without the bandwidth limitation, for each ring we get $\forall m \in [1, M] \quad f_m^{\max} = 8$ kHz. By adding the frequency restriction, some rings will have a lower value of $f_m^{\max}$, meaning that fewer microphones are required in the CRA.

Following the weight matrix modification, the FIR filters were designed for each ring using the MATLAB Signal Processing toolbox. The design process minimizes the integrated square error between the actual filter response and the ideal filter response [53]

$$\epsilon = \int_0^{\pi} \left(\hat{H}(\omega) - H(\omega) \right)^2 d\omega \,, \tag{4.20}$$

where ω is the normalized frequency, $\hat{H}(\omega)$ is the actual filter response and $H(\omega)$ is the ideal response. To maintain a fixed time delay, all the FIR filters were designed to have 32 coefficients each. The design process of the nonuniform constant beamwidth beamformer is summarised in Algorithm 4.1.

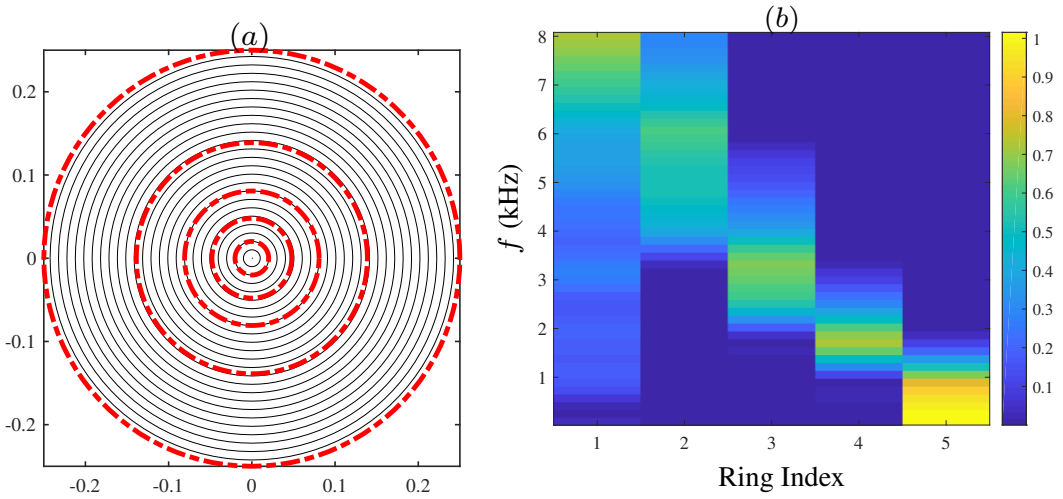

Figure 4.1: Constant beamwidth optimized NU-CRA beamformer. (a) Chosen rings (dashed-red) out of the optional radii grid. The grid was downsampled for visualization reasons. (b) Beamformer weight values applied to the array at each frequency.

4.3 Experimental Results

In this section, we compare the uniform beamformer (U-CRA) and the nonuniform beamformer (NU-CRA), both designed to attain constant elevation beamwidth while maximizing the DF. The results shown in this section are for CRA beamformers designed to attain the beamwidth of $\theta_{\text{BW}} = 30°$. The beamwidth is defined at the -3 dB amplitude, marked as β_{BW}. The number of the microphone elements in each ring is set according to (4.2) to prevent spatial aliasing. Note that for both beamformers the bandwidth limitation for each ring was applied. As described in Section 4.2.3, following the initial optimization, a pre-processing step was added, restricting each ring to be effective at specified frequency bands. The optimization problems shown in (4.17) and (4.19) were solved using MATLAB CVX toolbox [55]. Next, the filters were implemented in the time domain and applied to the CRAs. It should be mentioned that the computation time of the U-CRA beamformer is lower than the NU-CRA beamformer (depending on the grid size). However, the NU-CRA beamformer results in better performance measures as will be presented next.

The NU-CRA beamformer weights were calculated for a grid containing $N_{\text{R}} = 100$ equally spaced rings in the radii range $\underline{\boldsymbol{r}} \in [0, 25]$ cm. A set of $M = 5$ rings where selected from the problem solution at radii $\underline{\boldsymbol{r}}_{\text{opt}} = [2, 4.8, 8.1, 13.9, 25]$ cm, with approximately logarithmic scaling of 2, as shown in Fig. 4.1(a).

The resulting ring spacing is not linear, and the spacing between two adjacent rings is gradually growing from the inner ring to the outer rings. Figure 4.1(b) shows the beamformer weights. The y-axis represents frequency bins used for designing the array filters, and the x-axis represents the ring index (1-5), where index 1 is the inner-most ring. In the lower frequency range, the optimized solution includes solely the outer-most

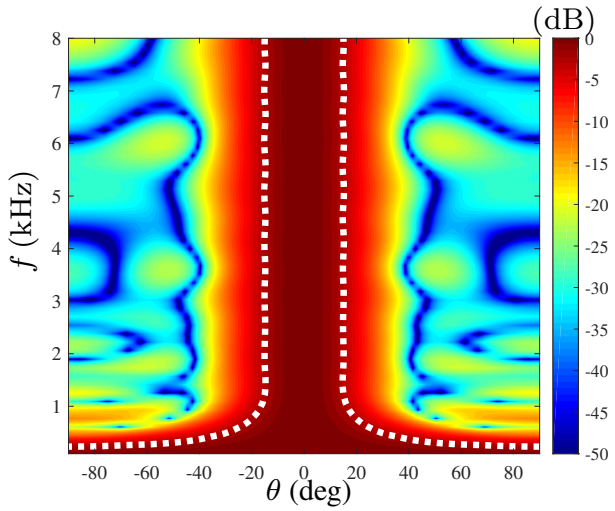

Figure 4.2: Beampattern of a 5-ring CRA, attenuated with the nonuniform beamformer filters. The dashed line marks the half-power (-3 dB) points of the main lobe.

ring. This selection is preferred for DF as the beamwidth of the outer ring is narrower in low frequencies than the remainder of the CRA rings. The relation between the ring radius and the beamwidth is evident from the properties of the zero-order Bessel function [51]. As the frequency increases, the beamforming is done by weighting the inner-most ring and one of the outer rings, gradually decreasing the outer rings' weight and minimizing the effective radius. Hence, by controlling the beampattern trade-off between the inner ring and a single ring beampattern with decreasing radius - the beamwidth is kept constant. In addition, the frequency responses of the FIR filters produced per ring are continuous and do not contain any irregularities.

The beampattern amplitude is shown in Fig. 4.2, with dashed lines highlighting the half-power (-3 dB) points of the main lobe. The beamwidth is maintained constant in the specified θ_{BW} over a range of frequencies $f \in [1, 8]$ kHz. Hence, the suggested constraints in problem (4.19) ensure a frequency-invariant beamwidth in the attainable frequency range. In addition, we note that the sidelobe level is low compared to the mainbeam (which is desired when the beamformer aims to maximize the DF).

As mentioned in Section 2.4, the DF and WNG are important characteristics of any beamformer. The main objective of the suggested beamformers was to gain maximal DF while maintaining fixed beamwidth. Thus, the DF as a function of frequency is presented in Fig. 4.3(a). While both beamformers attain constant beamwidth, compared to the U-CRA beamformer (dashed-triangle plot) the NU-CRA design (pointed-square plot) shows superior performance in frequencies where 4 kHz $< f$. The maximal difference between the beamformers is ≈ 10 dB in the DF. Due to the optimized selection of ring positions in the NU-CRA beamformer, the beampattern characteristics are preferred in terms of DF.

Figure 4.3(b) plots the WNG of the discussed beamformers. Note that in lower frequencies having $f <$ 0.6 kHz, the WNG of the NU-CRA is 1 dB higher compared

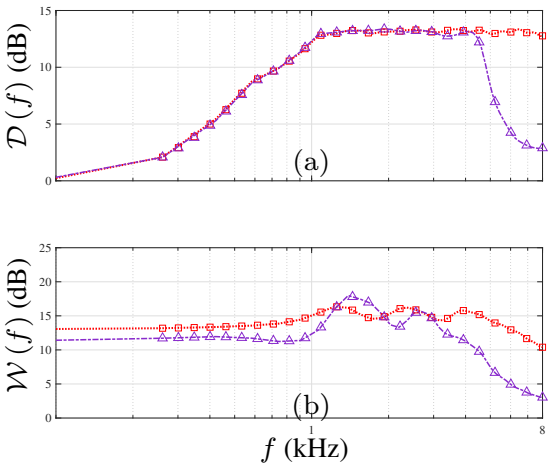

Figure 4.3: Performance measures for 5-ring U-CRA (dash-dot line with triangles) and NU-CRA (dotted line with squares) beamformers. (a) DF and (b) WNG, as a function of frequency. The x-axis is log-scaled for presentation.

to the U-CRA. In the lower frequency range, both beamformers include solely the outer-most ring. Since the outer ring in the NU-CRA is effective in higher frequencies compared to the U-CRA, it includes more microphone elements. As a result, the WNG of the NU-CRA in that frequency range is a bit higher. In higher frequencies, the NU-CRA presents higher WNG, with an average difference of 7 dB. The decrease of the WNG of the U-CRA beamformer at these frequencies is caused due to a high weight value given to the central microphone. In the U-CRA beamformer the rings are equally spaced in the range $\underline{\boldsymbol{r}} \in [0, 25]$ cm, meaning that the inner-most ring is a single microphone in the center of the array. The NU-CRA beamformer solution yielded the inner-most ring in $r = 2$ cm, constructed of 6 equally spaced microphones. As a result, the U-CRA depends on the central microphone, affecting the robustness of the array to microphone imperfections, which is reflected by the WNG.

To examine the dependency on the number of rings in the array, Fig. 4.4 presents the performance measures of the U-CRA and NU-CRA beamformers constructed of 4 rings (compared to the 5 rings array presented in Fig. 4.3). First, we note that the enhanced performance in terms of DF and WNG of the NU-CRA is consistent in the 4 ring constellation. Second, comparing Figs. 4.3(a) and 4.4(a) demonstrates an additional advantage of the NU-CRA beamformer: given a smaller number of rings, the improvement of the DF is established in lower frequencies. In Fig. 4.4(a) the NU-CRA DF is higher than the U-CRA starting from 3.1 kHz $< f$. In the 5 rings array, the improvement of the DF is noted from 4 kHz $< f$. Hence, when the number of rings is smaller, the frequency range in which the NU-CRA outperforms the U-CRA is wider, making the NU-CRA a preferable choice.

Out-of-beamwidth signals can interrupt and distort the output signal. The sidelobe attenuation can be helpful in the suppression of the noise signals and enhance the DF. Figure 4.5 shows the beampattern of the discussed beamformers at frequency

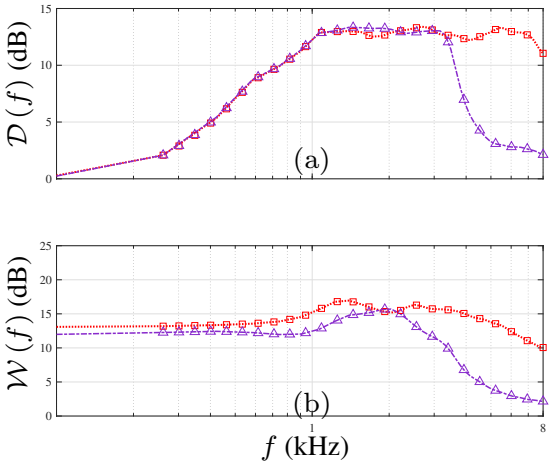

Figure 4.4: Performance measures for 4-ring U-CRA (dash-dot line with triangles) and NU-CRA (dotted line with squares) beamformers. (a) DF and (b) WNG, as a function of frequency.

$f = 5$ kHz. The frequency was chosen out of the frequency range in which the desired beamwidth is attained. There is a significant 24 dB difference in the first sidelobe level between the beamformers. The gap between the sidelobe levels is reflected in the DF comparison as discussed above. Additional frequencies in the range demonstrated corresponding relations between the sidelobe levels.

4.4 Summary

We have presented broadband beamforming methods for concentric circular arrays, which are broadly used in audio communication applications. The objective of the presented beamformers is to control the elevation beamwidth while optimizing the DF across a wide range of frequencies. The designs assume different degrees of freedom in the array geometry and the beamformer constraints. A constant beamwidth beamformer aiming to optimize the DF on a set of given ring radii was suggested. The incoherent optimization problem, solved for each frequency bin separately, and the constraints enabling a constant beamwidth were presented and applied on an equally spaced CRA. In addition, a coherent beamformer was proposed to sparsely select the optimal rings placements while simultaneously achieving the problem specifications. To ensure a joint selection of rings over the entire frequency range, a new set of constraints was presented employing the properties of a binary mask. Furthermore, to ensure the equal or higher performance of the sparse beamformer, the incoherent beamformer was utilized as a weighting coefficient in the coherent cost function.

The sparse optimization yielded a non-uniformly spaced CRA. Simulations show that the proposed coherent and incoherent beamforming methods attained comparable high directivity, yet the nonuniform beamformer outperforms the uniform beamformer. The advantages of the nonuniform beamformer were also shown for a different CRA

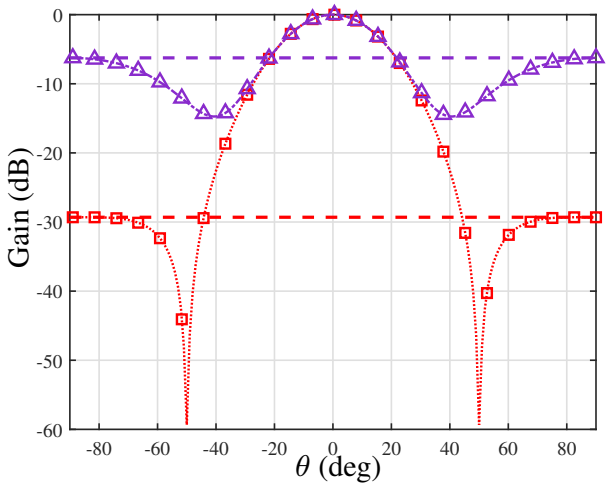

Figure 4.5: Beampattern for $f = 5000$ Hz calculated for U-CRA (dash-dot line with triangles) and NU-CRA (dotted line with squares) beamformers. The first sidelobe level of each beampattern is marked by a dashed line.

configuration, constructed of fewer rings. Hence, based on the design restrictions one can apply the suggested methodology to attain superior performance concerning the DF. The proposed beamformers apply the same filter to all the elements on each ring, resulting in reduced computational complexity in the design process and fewer resources in a physical setup. The computational complexity is a crucial factor in the convergence of the optimized solution. In addition, a limitation to the effective beamwidth of each ring in the CRA was suggested. The beamwidth limitation enabled the use of fewer microphones per ring while attaining the desired beampattern properties. A time-domain implementation of the ideal beamformer filters was presented and applied to the CRAs. Future research may focus on additional parameter optimizations, diverse array geometries, and numerical algorithms to solve the optimization problem.

Chapter 5

Conclusions

5.1 Summary

We have addressed the problem of constant-elevation beamwidth beamformers, applied on concentric ring arrays. The circular array geometry can be utilized in numerous 3-dimensional applications, including microphone arrays, sonar systems, and audio communication. However, existing methods mostly focus on the azimuth-beamwidth. The elevation beamwidth is also crucial in scenarios where the signal-of-interest has an arbitrary direction of arrival. Thus, eliminating the elevation direction may result in decreased performance of the beamformer. In the thesis, we present a system of multiple fixed beamforming areas, incorporating ceiling concentric ring arrays. In a system of such, the need for beam steering is eliminated and the area of interest can be covered by adjusting the desired elevation-beamwidth. A main advantage of the suggested system is the use of concentric ring arrays (compared to circular arrays). That is, when the need for beam steering is redundant, one can apply a joint attenuation value to all the sensors on each ring. This restriction significantly improves the computational complexity of the design, since the number of beamformer weights is determined by the number of rings in the array (rather than the number of sensors). In addition, the CRA configuration enables the use of fewer physical resources in a set-up. The signals captured by each sensor on a ring can be summed before sampling, resulting in a single A\D sampler per ring. Due to the presented advantages of the CRA configuration, we present in the thesis several constant beamwidth beamformers for CRAs.

In Chapter 3, a window-based beamformer is suggested. The beamformer is applied on a uniformly spaced set of rings and is designed to maintain a constant beamwidth over a wide range of frequencies. By analyzing the characteristics of a continuous ring beampattern and a rigid piston, we propose a gradual elimination beamforming algorithm. Hence, by gradually attenuating the outer rings as the frequency increases the beamwidth remains fixed. The attenuation magnitude for each frequency bin is calculated analytically and a precise form of the beamformers weights is presented. A modification to the lower frequency range is also presented in the thesis, enlarging the

effective frequency range for which the beamwidth is maintained. In low frequencies, we propose a gradual addition of inner rings as the frequency increases (starting from the outer-most ring). The modification decreased the minimal frequency for which the desired beamwidth is attained. Furthermore, a directivity index improvement is applied on the out-of-bound frequencies, as suggested in previous work on linear arrays. The different beamformers were implemented in the time-domain, using FIR filters with 36 coefficients for each ring. In the thesis, we show that the proposed design indeed maintains constant beamwidth over a broad frequency band. We also present the improvements in beamwidth consistency and directivity index by adding the suggested modifications. Moreover, the enhanced performance of the presented beamformer in terms of directivity index, white noise gain, and sidelobe attenuation is shown. We also examined the flexibility of the design to several desired beamwidths and explain the trade-off between the beamwidth and the minimal frequency for which it is attained.

In Chapter 4, we present an additional methodology in designing constant beamwidth CRA. However, opposed to the window-based beamformer, the presented designs do not assume any window shape for the beamformers weights. The proposed beamformer aims to maximize the directivity factor of the array while maintaining a constant beamwidth. To do so, we present two optimization problems yielding the beamformers' weights under different degrees of freedom. First, a uniformly spaced CRA with pre-defined ring locations is considered. In the proposed methodology a quadric optimization problem is defined. The cost function intends to maximize the directivity factor while the problem constraints obtain a constant beamwidth. In the case of the uniform CRA, the problem is solved for each frequency bin separately - resulting in the beamformers' weights. Second, a nonuniform CRA beamformer, which sparsely selects the rings' locations, is presented. Hence, by defining a modified optimization problem (performed coherently over the entire frequency range), the suggested methodology simultaneously selects the rings locations and yields the beamformers' weights. In addition, we incorporate the uniform solution in the cost function of the nonuniform optimization problem to ensure superior performance. The beamformers' weights were implemented in the time-domain by FIR filters. Simulation results show that the suggested constraints ensure a constant beamwidth beampattern for both beamformers. Moreover, we examine the beamformers' designs with respect to the directivity factor, white noise gain, and sidelobe attenuation. In all of the presented measurements, the nonuniform beamformer out-performs the uniform configuration. Nonetheless, simulations show that for CRAs with fewer rings the difference between the uniform and nonuniform beamformers is magnified. Thus, for arrays with a limited number of rings, the nonuniform solution is preferable.

5.2 Future Research

Throughout this thesis, we developed various approaches to obtain constant elevation beamwidth on CRAs. Although improved performance was obtained, as reflected from the simulations, there are still other issues for future research directions that can be conducted:

1. Our research focused on designing beamformers for the circular array geometry. However, this work can be expanded to volumetric arrays which incorporate sensors on a 3D volume rather than a 2D plane. Adding more degrees of freedom and additional dimension to be controlled can yield superior performance compared to the 2D geometry.

2. The spacing among adjacent sensors on each ring is considered uniform in this research. Several acoustic applications utilize logarithmic scales to simulate the mechanism of the human ear. Thus, it is of great interest to assimilate such prior knowledge in the sparse design resulting in optimized sensors locations. The number of sensors on each ring can also be incorporated as an optimization target.

3. The nonuniform beamformer was designed to maximize the directivity factor while maintaining a constant beamwidth. The directivity index maximization can be altered with a different cost function. Hence, several array properties can be optimized under the given constraints, such as sidelobe level, array gain, and more.

4. While outperforming the uniform CRA, the nonuniform beamformer includes higher computational complexity. Since the rings locations are sparsely selected out of a rigid grid and the optimization is conducted on the entire frequency range, the convergence time of the algorithm is significantly higher. Hence, solving the optimization problem using advanced numerical methods may be of interest for real-time applications with varying set-up.

Bibliography

[1] B. D. V. Veen and K. M. Buckley, "Beamforming: A versatile approach to spatial filtering," *IEEE ASSP Mag.*, vol. 52, pp. 4–24, 1988.

[2] M. Brandstein and D. Ward, eds., *Microphone Arrays: Signal Processing Techniques and Applications*. Digital signal processing, New York: Springer, 2001.

[3] C. A. Balanis, *Antenna Theory: Analysis and Design*. Hoboken, New Jersey: Wiley, fourth edition ed., 2016.

[4] H. L. Van-trees, *Detection, Estimation and Modulation Theory, Part IV - Optimum Array Processing*. New York: Wiley Interscience, 2002.

[5] J. Benesty, I. Cohen, and J. Chen, *Fundamentals of Signal Enhancement and Array Signal Processing*. Singapore: Wiley-IEEE Press, 2018.

[6] D. B. Ward, R. A. Kennedy, and R. C. Williamson, "Theory and design of broadband sensor arrays with frequency invariant far-field beam patterns," *The Journal of the Acoustical Society of America*, vol. 97, pp. 1023–1034, Feb. 1995.

[7] T. Chou, "Frequency-independent beamformer with low response error," in *Proc. of International Conference on Acoustics, Speech, and Signal Processing*, vol. 5, (Detroit, MI, USA), pp. 2995–2998, IEEE, 1995.

[8] S. Gannot, D. Burshtein, and E. Weinstein, "Signal enhancement using beamforming and nonstationarity with applications to speech," *IEEE Transactions on Signal Processing*, vol. 49, pp. 1614–1626, Aug. 2001.

[9] Wei Liu and S. Weiss, "New class of broadband arrays with frequency invariant beam patterns," in *Proc. IEEE International Conference on Acoustics, Speech, and Signal Processing*, vol. 2, (Montreal, Que., Canada), pp. ii–185–8, IEEE, 2004.

[10] S. Markovich, S. Gannot, and I. Cohen, "Multichannel eigenspace beamforming in a reverberant noisy environment with multiple interfering speech signals," *IEEE Transactions on Audio, Speech, and Language Processing*, vol. 17, pp. 1071–1086, Aug. 2009.

[11] W. Liu, "Adaptive wideband beamforming with sensor delay-lines," *Signal Processing*, vol. 89, pp. 876–882, May 2009.

[12] M. Crocco and A. Trucco, "Design of robust superdirective arrays with a tunable tradeoff between directivity and frequency-invariance," *IEEE Transactions on Signal Processing*, vol. 59, pp. 2169–2181, May 2011.

[13] Z. Yong and L. Wei, "Robust fixed frequency invariant beamformer design subject to norm-bounded errors," *IEEE Signal Processing Letters*, vol. 20, pp. 169–172, Feb. 2013.

[14] R. Berkun, I. Cohen, and J. Benesty, "Combined beamformers for robust broadband regularized superdirective beamforming," *IEEE/ACM Transactions on Audio, Speech, and Language Processing*, pp. 877–886, 2015.

[15] J. Benesty, I. Cohen, and J. Chen, *Fundamentals of Signal Enhancement and Array Signal Processing*. Hoboken, NJ: John Wiley & Sons, 2018.

[16] W. P. M. N. Keizer, "Fast low-sidelobe synthesis for large planar array antennas utilizing successive fast Fourier transforms of the array factor," *IEEE Transactions on Antennas and Propagation*, vol. 55, pp. 715–722, Mar. 2007.

[17] L. Manica, P. Rocca, and A. Massa, "Design of subarrayed linear and planar array antennas with sll control based on an excitation matching approach," *IEEE Transactions on Antennas and Propagation*, vol. 57, no. 6, pp. 1684–1691, 2009.

[18] J. Wu, W. N. Huang, Y. J. Cheng, and Y. Fan, "A broadband high-gain planar array antenna for V-band wireless communication," in *Proc. of 3rd Asia-Pacific Conference on Antennas and Propagation*, (Harbin, China), pp. 309–312, IEEE, July 2014.

[19] C. Mathews and M. Zoltowski, "Eigenstructure techniques for 2-d angle estimation with uniform circular arrays," *IEEE Transactions on Signal Processing*, vol. 42, pp. 2395–2407, 1994.

[20] P. Ioannides and C. Balanis, "Uniform circular arrays for smart antennas," *IEEE Antennas and Propagation Magazine*, vol. 47, no. 4, pp. 192–206, 2005.

[21] E. Tiana-Roig, F. Jacobsen, and E. F. Grande, "Beamforming with a circular microphone array for localization of environmental noise sources," *The Journal of the Acoustical Society of America*, vol. 128, pp. 3535–3542, 2010.

[22] A. M. Torres, M. Cobos, B. Pueo, and J. J. Lopez, "Robust acoustic source localization based on modal beamforming and time–frequency processing using circular microphone arrays," *The Journal of the Acoustical Society of America*, vol. 132, pp. 1511–1520, Sept. 2012.

[23] S. Yan, "Optimal design of modal beamformers for circular arrays," *The Journal of the Acoustical Society of America*, vol. 138, pp. 2140–2151, Oct. 2015.

[24] Y. Li, K. Ho, and C. Kwan, "Beampattern synthesis for concentric circular ring array using mmse design," *IEEE Proc. Circuits and Systems Int. Symp.*, pp. 329––332, 2004.

[25] X. Zhao, Q. Yang, and Y. Zhang, "A hybrid method for the optimal synthesis of 3-d patterns of sparse concentric ring arrays," *IEEE Transactions on Antennas and Propagation*, vol. 64, pp. 515–524, 2016.

[26] Y. Wang and Y.Yang, "A flexible method for designing frequency-invariant beamformers with circular sensor arrays," *IEEE Access*, vol. 6, pp. 57073–57084, Sep 2018.

[27] S. Chan and H. Chen, "Uniform concentric circular arrays with frequency invariant characteristics – theory, design, adaptive beamforming and doa estimation," *IEEE Trans. Signal Process.*, vol. 50, pp. 165–177, 2007.

[28] H. H. Chen, S. C. Chan, Z. G. Zhang, and K. L. Ho, "Adaptive beamforming and recursive doa estimation using frequency-invariant uniform concentric spherical arrays," *IEEE Transactions on Circuits and Systems I: Regular Papers*, vol. 55, no. 10, pp. 3077–3089, 2008.

[29] Y. Zhao, W. Liu, and R. Langley, "Application of the least squares approach to fixed beamformer design with frequency-invariant constraints," *IET Signal Processing*, vol. 5, p. 281, 2011.

[30] Y. Buchris, A. Amar, J. Benesty, and I. Cohen, "Incoherent synthesis of sparse arrays for frequency-invariant beamforming," *IEEE/ACM Transactions on Audio, Speech, and Language Processing*, vol. 27, pp. 482–495, 2019.

[31] Y. Buchris, I. Cohen, J. Benesty, and A. Amar, "Joint sparse concentric array design for frequency and rotationally invariant beampattern," *IEEE/ACM Transactions on Audio, Speech, and Language Processing*, vol. 28, pp. 1143–1158, 2020.

[32] J. Benesty, J. Chen, and I. Cohen, *Design of Circular Differential Microphone Arrays*, vol. 12 of *Springer Topics in Signal Processing*. Cham: Springer International Publishing, 2015.

[33] G. Huang, J. Benesty, and J. Chen, "Design of robust concentric circular differential microphone arrays," *The Journal of the Acoustical Society of America*, vol. 141, pp. 3236–3249, May 2017.

[34] Y. Buchris, I. Cohen, and J. Benesty, "Asymmetric beampatterns with circular differential microphone arrays," in *Proc. WASPAA*, (New Paltz, NY), pp. 190–194, Oct. 15–18, 2017.

[35] G. Huang, J. Chen, and J. Benesty, "A flexible high directivity beamformer with spherical microphone arrays," *The Journal of the Acoustical Society of America*, vol. 143, pp. 3024–3035, May 2018.

[36] G. Huang, J. Chen, and J. Benesty, "Insights into frequency-invariant beamforming with concentric circular microphone arrays," *IEEE/ACM Trans. Audio, Speech, Language Process.*, vol. 26, pp. 2305–2318, 2018.

[37] Y. Yang, C. Sun, and C. Wan, "Theoretical and experimental studies on broadband constant beamwidth beamforming for circular arrays," in *Proc. Int. Conf. Oceans*, vol. 3, pp. 1647–1653, 2003.

[38] X. Zhang, W. Ser, and K. Muralidhar, "Uniform circular broadband beamformer with selective frequency and spatial invariant region," in *Proc. IEEE International Symposium on Circuits and Systems*, pp. 2201–2204, 2009.

[39] X. Zhang, W. Ser, Z. Zhang, and A. Krishna, "Selective frequency invariant uniform circular broadband beamformer," *EURASIP Journal on Advances in Signal Processing*, vol. 2010, p. 678306, Dec. 2010.

[40] J. Wang, Q. Feng, R. Wu, and Z. Su, "A constant-beamwidth beamforming method for acoustic imaging," in *Proc. of IEEE Antennas and Propagation Society International Symposium*, (Honolulu, HI), pp. 4236–4239, IEEE, June 2007.

[41] S. Li, X. Yang, L. Ning, T. Long, and T. K. Sarkar, "Broadband constant beamwidth beamforming for suppressing mainlobe and sidelobe interferences," in *Proc. of IEEE Radar Conference (RadarConf)*, (Seattle, WA, USA), pp. 1041–1045, IEEE, May 2017.

[42] O. Rosen, I. Cohen, and D. Malah, "FIR-based symmetrical acoustic beamformer with a constant beamwidth," *Signal Processing*, vol. 130, pp. 365–376, Jan. 2017.

[43] T. Long, I. Cohen, B. Berdugo, Y. Yang, and J. Chen, "Window-based constant beamwidth beamformer," *Sensors*, vol. 19, p. 2091, May 2019.

[44] R. Sharma, I. Cohen, and B. Berdugo, "Controlling elevation and azimuth beamwidths with concentric circular microphone arrays," *IEEE/ACM Transactions on Audio, Speech, and Language Processing*, vol. 29, pp. 1491–1502, 2021.

[45] R. Sharma, I. Cohen, and B. Berdugo, "Window beamformer for sparse concentric circular array," in *ICASSP 2021 - 2021 IEEE International Conference on Acoustics, Speech and Signal Processing (ICASSP)*, pp. 4500–4504, 2021.

[46] J. L. Flanagan, J. D. Johnston, R. Zahn, , and G. W. Elko, "Computer steered microphone arrays for sound transduction in large rooms," *J. Acoust. Soc. Am*, vol. 78, pp. 1508–1581, 1985.

[47] N. D. Gaubitch and P. A. Naylor, "Analysis of the dereverberation performance of microphone arrays," in *Proc. IEEE International Workshop on Acoustic Signal Enhancement*, (Eindhoven, The Netherlands), Sep 12–15 2015.

[48] D. Pinchera, "On the trade-off between the main parameters of planar antenna arrays," *Electronics*, vol. 9, pp. 739–758, 2020.

[49] A. Beck, *Introduction to Nonlinear Optimization: Theory, Algorithms, and Applications with MATLAB*. MOS-SIAM series on optimization, Philadelphia: Society for Industrial and Applied Mathematics : Mathematical Optimization Society, 2014.

[50] Yunhong Li, K. C. Ho, and C. Kwan, "3-D array pattern synthesis with frequency invariant property for concentric ring array," *IEEE Transactions on Signal Processing*, vol. 54, pp. 780–784, Feb. 2006.

[51] C. T. Molloy, "Calculation of the directivity index for various types of radiators," *The Journal of the Acoustical Society of America*, vol. 20, pp. 387–405, July 1948.

[52] R. A. Mucci and R. G. Pridham, "Comparison of shifted sideband and conventional beamforming techniques," *The Journal of the Acoustical Society of America*, vol. 65, pp. S61–S61, June 1979.

[53] A. V. Oppenheim, R. W. Schafer, and J. R. Buck, *Discrete-Time Signal Processing*. Upper Saddle River, NJ: Prentice Hall, 1999.

[54] D. P. Scholnik and J. O. Coleman, "Formulating wideband array-pattern optimization," in *Proc. IEEE Int. Conf. on Phased Array Systems and Technology*, (Dana Point, CA), pp. 489–492, May 2000.

[55] M. Grant, S. Boyd, and Y. Ye, "CVX: Matlab software for disciplined convex programming," 2008.

בנוסף לפתרון זה אנו מציגים מעצב אלומה עם רוחב קבוע על מערך טבעות בעל מרווחים לא אחידים. ברוב השיטות המוצגות בספרות המרווחים בין טבעות עוקבות הם אחידים. בניגוד לשיטות אלו, מעצב האלומה המוצג בחלק זה בוחר סימולטנית את מיקומי הטבעות (שאינם בהכרח במרחקים זהים) ומחשב את משקל הניחות לכל טבעת. תכנון מעצב האלומה מתבצע על ידי פתרון בעיית אופטימיזציה ייעודית. כלומר, מטרת מעצב האלומה המחושב הינה למקסם את מדד הכיווניות של המערך תוך שמירה על רוחב אלומה קבוע. בעבודה זו אנו מציגים את פונקציית המטרה ואילוצי הבעיה אשר מובילים למעצב האלומה הרצוי. בנוסף, אנו משלבים בפונקציית המטרה משקול בין התדרים על ידי שילוב של מעצב אלומה שתוכנן על מערך עם מיקומים אחידים. על ידי משקול זה מתקבלים עבור המערך שאיננו אחיד ביצועים המתעלים על המערך האחיד. תוצאות הסימולציה מעידות על עדיפותו של המערך הלא אחיד על פני מערך אחיד במגוון פרמטרי השוואה. באופן דומה לשיטה מבוססת החלון, גם עבור שיטה זו אנו מממשים את פונקציית המשקל במישור הזמן על ידי מסנני תגובת הלם סופית

תקציר

מערכות תקשורת, דימות רפואי, רדאר ויישומי דיבור מצריכים עיבוד של אותות רחבי סרט. מאחר והתווך האקוסטי כולל תופעות דוגמת רעשים והדהודים, חילוץ אות באיכות מיטבית במערכות הללו מהווה משימה מאתגרת. מעצבי אלומה רחבי סרט באים לידי שימוש במשימות רבות דוגמת שיפור האות, זיהוי כיון הגעתו והנחתת הרעשים הנלווים. עיצוב אלומת הכניסה מתבצע על ידי שינוי המשקל הניתן לאות הנקלט מחיישנים שונים במעצב האלומה, במטרה לגשר על הפערים האפשריים בתווך האקוסטי. מרכיב מהותי נוסף במעצב האלומה הוא מבנה מערך החיישנים הנבחר. בבעיות תלת מימדיות המערך הדו-מימדי טומן בחובו יתרונות משמעותיים ביחס למערכים חד מימדיים.

אחד האתגרים המשמעותיים בתכנון מעצב אלומה רחב סרט הינו שמירה על רוחב אלומה קבוע על פני טווח רחב של תדרים. במעצבי אלומה נפוצים, רוחב האלומה נעשה צר יותר עם העלייה בתדר. היצרות האלומה הראשית יכולה להוביל לעיוותים באות המוצא ולשינויים לא קונסיסטנטיים בין תדרים. על מנת להמנע מעיוות האות, מספר שיטות למעצבי אלומה הוצגו בספרות לאורך השנים. עם זאת, מרבית השיטות מתייחסות בעיקר לרוחב האלומה בכיוון האזימוטלי של הגעת האות (תוך התעלמות מכיוון העילוי). ביישומים תלת מימדיים מעשיים, הנחה זו יכולה להוביל לביצועים פחותים של מעצב האלומה במדד הכיווניות ובהגברת רעש לבן. בעבודה זו מוצגות מספר שיטות לתכנון מעצבי אלומה בעלי רוחב אלומה קבוע בכיוון העילוי. מעצבי אלומה אלו מתוכננים למערכים מעגליים קונצנטריים. בתצורת המערכים הנידונה בעבודה זו, אנו מוסיפים אילוץ לפיו כלל החיישנים על כל מערך מעגלי מונחתים באותו משקל. אילוץ זה מפחית משמעותית את כמות המשאבים החומרתיים הדרושים לתכנון המערך. בנוסף, האילוץ מקטין את הסיבוכיות החישובית בעת תכנון משקלי מעצב האלומה.

בהסתמך על שיטות מוכרות בפתרונות חד-מימדיים, עיצוב האלומה עם רוחב קבוע נעשה באמצעות תכנון פונקציית חלון ייעודית. על ידי ניתוח מאפייני האלומה של טבעת חיישנים, היחס בין רוחב האלומה, רדיוס המערך והתדר מחושב. בהתאם לכך, על ידי הנחתה הדרגתית של הטבעות החיצוניות אנו מחשבים את עוצמת ההנחתה המדויקת עבור כל תדר כל שיתקבל רוחב אלומה קבוע. ניחות הדרגתי זה משמר את היחס בין התדר לרדיוס המערך כך שרוחב האלומה נשמר. בנוסף לניחות הטבעות בתדרים גבוהים, אנו מציעים שיטה להרחבת רוחב הסרט בו רוחב האלומה נשמר בתדרים הנמוכים. בשינוי זה תצורת החלון המופעל על כל טבעת משתנה ממסנן מעביר נמוכים למסנן מעביר פס. כלומר, ע"י ניצול המאפיינים התיאורתיים של תצורת האלומה של טבעת חיישנים, מעצב האלומה המחושב מתעלה על פתרונות לינאריים עם מספר ערוצים זהה. בנוסף לשינוי תצורת החלון אנו מציגים את מימוש המשקולות התיאורטיים ע"י שימוש במסנני תגובת הלם סופית במרחב הזמן. ביצועי מעצב האלומה על בסיס פרמטרי איכות שונים התעלו על מעצב אלומה חד מימדי מסדר זהה.

המחקר בוצע בהנחייתם של פרופסור ישראל כהן וד"ר ברוך ברדוגו בפקולטה להנדסת חשמל ומחשבים.

התוצאות בחיבור זה פורסמו כמאמרים מאת המחבר ושותפיו למחקר בכנסים ובכתבי-עת במהלך תקופת מחקר המגיסטר של המחבר, אשר גרסאותיהם העדכניות ביותר הינן:

Avital Kleiman, Israel Cohen, and Baruch Berdugo. Constant-beamwidth beamforming with concentric ring arrays. *Sensors, special issue on Sensors in Indoor Positioning Systems*, 21:7253—7271, November 2021.

Avital Kleiman, Israel Cohen, and Baruch Berdugo. Constant-beamwidth nonuniform concentric ring microphone arrays. *IEEE/ACM Transactions on Audio, Speech, and Language Processing*, 2022 submitted.

תודות

עבודה זו נעשתה תחת הנחייתם של פרופסור ישראל כהן וד"ר ברוך ברדוגו בפקולטה להנדסת חשמל ומחשבים.

ברצוני להביע הוכרת תודה עמוקה למנחיי, פרופסור ישראל כהן וד"ר ברוך ברדוגו, על הנחייתם ותמיכתם לאורך המחקר. הודות לליווי הצמוד זכיתי ללמוד רבות ולרכוש כלים חדשים ועל כך הערכתי הרבה.

לבסוף, ברצוני להודות למשפחתי ולבן זוגי מתן על תמיכתם בתהליך זה. לא יכולתי להגיע להישג זה בלעדיהם.

אני מודה לטכניון, לתוכנית המחקר המשותפת של הקרן הלאומית למדע והקרן הלאומית למדעי הטבע של סין (מענק מס' 2514/17), ולקרן פזי על התמיכה הכספית הנדיבה בהשתלמותי.

תכן אופטימלי של מעצבי אלומה לרוחב אונה ראשית קבועה עם מערכים מעגליים קונצנטרים

חיבור על מחקר

לשם מילוי חלקי של הדרישות לקבלת התואר
מגיסטר למדעים בהנדסת חשמל

אביטל קליימן

הוגש לסנט הטכניון — מכון טכנולוגי לישראל
ניסן התשפ"ב חיפה אפריל 2022

תכן אופטימלי של מעצבי אלומה לרוחב אונה ראשית קבועה עם מערכים מעגליים קונצנטרים

אביטל קליימן